Repetitive Patterns in Rapid Optical Variations in the Nearby Black-hole Binary V404 Cygni

Mariko Kimura[1], Keisuke Isogai[1], Taichi Kato[1], Yoshihiro Ueda[1], Satoshi Nakahira[2], Megumi Shidatsu[3], Teruaki Enoto[1,4], Takafumi Hori[1], Daisaku Nogami[1], Colin Littlefield[5], Ryoko Ishioka[6], Ying-Tung Chen[6], Sun-Kun King[6], Chih-Yi Wen[6], Shiang-Yu Wang[6], Matthew J. Lehner[6,7,8], Megan E. Schwamb[6], Jen-Hung Wang[6], Zhi-Wei Zhang[6], Charles Alcock[8], Tim Axelrod[9], Federica B. Bianco[10], Yong-Ik Byun[11], Wen-Ping Chen[12], Kem H. Cook[6], Dae-Won Kim[13], Typhoon Lee[6], Stuart L. Marshall[14], Elena P. Pavlenko[15], Oksana I. Antonyuk[15], Kirill A. Antonyuk[15], Nikolai V. Pit[15], Aleksei A. Sosnovskij[15], Julia V. Babina[15], Aleksei V. Baklanov[15], Alexei S. Pozanenko[16,17], Elena D. Mazaeva[16], Sergei E. Schmalz[18], Inna V. Reva[19], Sergei P. Belan[15], Raguli Ya. Inasaridze[20], Namkhai Tungalag[21], Alina A. Volnova[16], Igor E. Molotov[22], Enrique de Miguel[23,24], Kiyoshi Kasai[25], William Stein[26], Pavol A. Dubovsky[27], Seiichiro Kiyota[28], Ian Miller[29], Michael Richmond[30], William Goff[31], Maksim V. Andreev[32,33], Hiromitsu Takahashi[34], Naoto Kojiguchi[35], Yuki Sugiura[35], Nao Takeda[35], Eiji Yamada[35], Katsura Matsumoto[35], Nick James[36], Roger D. Pickard[37,38], Tamás Tordai[39], Yutaka Maeda[40], Javier Ruiz[41,42,43], Atsushi Miyashita[44], Lewis M. Cook[45], Akira Imada[46] & Makoto Uemura[47]

[1]*Department of Astronomy, Graduate School of Science, Kyoto University, Oiwakecho, Kitashirakawa, Sakyo-ku, Kyoto 606-8502, Japan*

[2]*JEM Mission Operations and Integration Center, Human Spaceflight Technology Directorate, Japan Aerospace Exploration Agency, 2-1-1 Sengen, Tsukuba, Ibaraki 305-8505, Japan*

[3]*MAXI team, RIKEN, 2-1 Hirosawa, Wako, Saitama 351-0198, Japan*

[4]The Hakubi Center for Advanced Research, Kyoto University, Kyoto 606-8302, Japan

[5]Astronomy Department, Wesleyan University, Middletown, CT 06459 USA

[6]Institute of Astronomy and Astrophysics, Academia Sinica, 11F of Astronomy-Mathematics Building, AS/NTU. No.1, Sec. 4, Roosevelt Rd, Taipei 10617, Taiwan (R.O.C.)

[7]Department of Physics and Astronomy, University of Pennsylvania, 209 S. 33rd St., Philadelphia, PA 19125, USA

[8]Harvard-Smithsonian Center for Astrophysics, 60 Garden St, Cambridge, MA 02138, USA

[9]Steward Observatory, University of Arizona, Tucson, Arizona 85721, USA

[10]Center for Cosmology and Particle Physics, New York University, 4 Washington Place, New York, New York 10003, USA

[11]Department of Astronomy and University Observatory, Yonsei University, Seoul 120-749, Korea

[12]Institute of Astronomy and Department of Physics, National Central University, Chung-Li 32054, Taiwan (R.O.C.)

[13]Max Planck Institute for Astronomy, Knöigstuhl 17, 69117 Heidelberg, Germany

[14]Kavli Institute for Particle Astrophysics and Cosmology (KIPAC), Stanford University, 452 Lomita Mall, Stanford, California 94309, USA

[15]Crimean Astrophysical Observatory, 298409, Nauchny, Republic of Crimea

[16]Space Research Institute, Russian Academy of Sciences, 117997 Moscow, Russia

[17]National Research Nuclear University MEPhI (Moscow Engineering Physics Institute), Moscow, Russia

[18]Leibniz Institute for Astrophysics, Potsdam, Germany

[19]*Fesenkov Astrophysical Institute, Almaty, Republic of Kazakhstan*

[20]*Kharadze Abastumani Astrophysical Observatory, Ilia State University, Tbilisi, Georgia*

[21]*Center of Astronomy and Geophysics Mongolian Academy of Sciences, Ulaanbaatar, Mongolia*

[22]*Keldysh Institute of Applied Mathematics, Russian Academy of Sciences, Moscow, Russia*

[23]*Departamento de Física Aplicada, Facultad de Ciencias Experimentales, Universidad de Huelva, 21071 Huelva, Spain*

[24]*Center for Backyard Astrophysics, Observatorio del CIECEM, Parque Dunar, Matalascañas, 21760 Almonte, Almonte, Huelva, Spain*

[25]*Baselstrasse 133D, CH-4132 Muttenz, Switzerland*

[26]*6025 Calle Paraiso, Las Cruces, New Mexico 88012, USA*

[27]*Vihorlat Observatory, Mierova 4, Humenne, Slovakia*

[28]*Variable Star Observers League in Japan (VSOLJ), 7-1 Kitahatsutomi, Kamagaya, Chiba 273-0126*

[29]*Furzehill House, Ilston, Swansea, SA2 7LE, UK*

[30]*Physics Department, Rochester Institute of Technology, Rochester, New York 14623, USA*

[31]*American Association of Variable Star Observers (AAVSO), 13508 Monitor Lane Sutter Creek, CA 95685*

[32]*Institute of Astronomy, Russian Academy of Sciences, 361605 Peak Terskol, Kabardino-Balkaria, Russia*

[33]*International Center for Astronomical, Medical and Ecological Research of National Academy of Sciences of Ukraine (NASU), 27 Akademika Zabolotnoho str., 03680 Kiev, Ukraine*

3

[34] *Department of Physical Science, School of Science, Hiroshima University, 1-3-1 Kagamiyama, Higashi-Hiroshima, Hiroshima 739-8526, Japan*

[35] *Osaka Kyoiku University, 4-698-1 Asahigaoka, Kashiwara, Osaka 582-8582, Japan*

[36] *1 Tavistock Road, Chelmsford, Essex, CM1 6JL, UK*

[37] *The British Astronomical Association, Variable Star Section (BAA VSS), Burlington House, Piccadilly, London, W1J 0DU, UK*

[38] *3 The Birches, Shobdon, Leominster, Herefordshire, HR6 9NG, UK*

[39] *Polaris Observatory, Hungarian Astronomical Association, Laborc utca 2/c, 1037 Budapest, Hungary*

[40] *112-14 Kaminishiyama-machi, Nagasaki, Nagasaki 850-0006, Japan*

[41] *Observatorio de Cantabria, Ctra. de Rocamundo s/n, Valderredible, Cantabria, Spain*

[42] *Instituto de Fisica de Cantabria (CSIC-UC), Avenida Los Castros s/n, E-39005 Santander, Cantabria, Spain*

[43] *Agrupacion Astronomica Cantabra, Apartado 573, 39080, Santander, Spain*

[44] *Seikei Meteorological Observatory, Seikei High School, Kichijoji-kitamachi 3-10-13, Musashino, Tokyo 180-8633, Japan*

[45] *Center for Backyard Astrophysics (Concord), 1730 Helix Ct. Concord, California 94518, USA*

[46] *Kwasan and Hida Observatories, Kyoto University, Kitakazan-Ohmine-cho, Yamashina-ku, Kyoto, Kyoto 607-8471, Japan*

[47] *Hiroshima Astrophysical Science Center, Hiroshima University, Kagamiyama 1-3-1, Higashi-Hiroshima, Hiroshima 739-8526, Japan*

How black holes accrete surrounding matter is a fundamental, yet unsolved question in astrophysics. It is generally believed that when the mass accretion rate approaches the critical rate (Eddington limit), thermal instability occurs in the inner disc, causing repetitive patterns[1] of violent X-ray variability (oscillations) on timescales of minutes to hours. In fact, such oscillations have been observed only in high mass accretion rate sources, like GRS 1915+105[2,3]. These phenomena are thought to have distinct physical origins from X-ray or optical variations with much smaller amplitudes and faster ($\lesssim$10 sec) timescales often observed in other black hole binaries (e.g., XTE J1118+480[4] and GX 339−4[5]). Here we report an extensive multi-colour optical photometric dataset of V404 Cygni, an X-ray transient[6] containing a black hole of nine solar masses[7] at a distance of 2.4 kpc[8]. Our data show that optical oscillations on timescales of 100 sec to 2.5 hours can occur at mass accretion rates >10 times lower than previously thought[1]. This suggests that the accretion rate is not the critical parameter for inducing inner disc instabilities. Instead, we propose that a long orbital period is a key condition for these phenomena, because the outer part of the large disc in binaries with long orbital periods will have surface densities too low to maintain the sustained mass accretion to the inner part of the disc. The lack of sustained accretion – not the actual rate – would then be the critical factor causing violent oscillations in long-period systems.

V404 Cyg, which was originally discovered as a nova in 1938 and detected by the GINGA satellite in 1989[9], underwent an outburst in 2015 June after 26 years of dormancy. At 18:31:38 on June 15 (15.77197 Universal Time (UT)), Swift/Burst Alert Telescope (BAT) initially detected this outburst as a possible gamma-ray burst[10]. The outburst was also detected by the Monitor of

All-sky X-ray Image (MAXI) instrument on June 16.783 UT[11].

Following these detections, we started a world-wide photometric campaign (Extended Data Tables 1 and 2, Sec. 1 of Methods) partly within the Variable Star Network (VSNET) Collaboration, and collected extensive sets of multi-colour optical photometric data consisting of >85,000 points. Our dataset also includes early observations with the Taiwanese-American Occultation Survey (TAOS) starting on June 15, 18:34:07 UT, 2 min 29 sec after the Swift/BAT trigger[12] (Extended Data Tables 1 and 2, Sec. 1 of Methods on the VSNET collaboration team and TAOS). Some weak activity started approximately 1,000 s before the Swift/BAT trigger[13]. The same activity above 80 keV was also detected by the active anti-coincidence shield (ACS) of Spectrometer on INTEGRAL (SPI) telescope of INTEGRAL observatory in the same time intervals (P. Minaev, private communication).

Our observations immediately indicated that large-amplitude short-term variations on timescales of $\sim$100 s to $\sim$2.5 hours were already present, starting less than three minutes after the Swift/BAT trigger. In Fig. 1 and Extended Data Fig. 1, we show the overall optical multi-colour light curves. The overall trend of the light curves can be divided into three stages: (1) gradual rise during BJD (Barycentric Julian Day) 2,457,189–2,457,194.5 (brightening by 1 mag d^{-1} on average), (2) the plateau during BJD 2,457,194.5–2,457,200.0, and (3) rapid fading during BJD 2,457,200.0–2,457,203.3 (fading on average by 2.5 mag d^{-1}). Short-term variations with amplitudes varying between 0.1–2.5 mag were observed throughout the outburst and consisted of characteristic structures such as recurrent sudden dips from a peak (Fig. 1).

Moreover, fluctuations similar in shapes to the unique X-ray variations of the enigmatic black hole binary GRS 1915+105[2] are present in the optical light curve of V404 Cyg (Fig. 2). The patterns in the X-ray light curve of GRS 1915+105 have been classified into at least 12 classes on the basis of their flux and colour characteristics[3]. Repeating structures like these had not been observed in optical wavelengths prior to the 2015 outburst of V404 Cyg. The variations that we observed can be divided into two characteristic classes: (1) dip-type oscillations (repetitions of a gradual rise followed by a sudden dip, sometimes with accompanying spikes on timescales of ∼45 min–∼2.5 hours; Fig. 2a, b, and c) and (2) heartbeat-type oscillations (rhythmic small spikes with short periods of ∼5 min; Fig. 2d). Although rapid optical variations have been detected in the black hole binary V4641 Sgr, the variations are stochastic with no indication of regular patterns[14]. The variations we found in V404 Cyg at optical wavelengths were regular and similar in shape to those in GRS 1915+105, although the interval between dips is about 5 times larger in V404 Cyg than in GRS 1915+105.

Using X-ray data from Swift/X-ray Telescope (XRT), we compared simultaneous optical and X-ray light curves (Fig. 3). When both X-ray and optical data showed strong short-term variations, the correlations were generally good, although the X-ray flux variations are much larger than the optical ones. The good correlation indicates that both X-ray and optical observations recorded the same phenomena (see also Sec. 2 in Methods and Extended Data Fig. 2). Spectral analyses of the simultaneous X-ray data (Sec. 3 in Methods and Extended Data Fig. 3) indicate that there was no tendency for increased absorption when the X-ray flux decreased, suggesting that these dips do not originate in absorption. In some epochs, we found evidence for heavy obscuration as found in the

GINGA data during the 1989 outburst[15]; however this is not related to dip-type variations. We can thus infer that the short-term fluctuations directly reflect variations in radiation from the accretion disc or its associated structures. Detailed analyses of the typical simultaneous broad-band spectral energy distribution (SED) (Sec. 8 of Methods and Extended Data Fig. 6) show that the majority of the optical flux is most likely produced by reprocessing of X-ray irradiation in the disc.

In GRS 1915+105, it has been proposed that the observed variability is caused by limit-cycle oscillations in the inner accretion disc due to the Lightman-Eardley viscous instability[16], which can explain a slow rise in brightness (mass accumulation) followed by a sudden drop (accretion to the black hole). Such a model assumes that the black hole is accreting mass nearly at the Eddington rate, which is supported by observations of GRS 1915+105[17]. Similar types of X-ray variability have also been detected in the black hole binary IGR J17091−3624[18], whose Eddington rate is unknown because both the mass and the distance are uncertain.

In V404 Cyg, however, the accurate determination of the distance based on a parallax measurement[8] and the dynamical mass determination[7] enable us to conclude from our 2015 data that the black hole in this system was accreting at much lower rate than the Eddington rate most of the time. During the period when GRS 1915+105-type variations in the optical light curves were recorded in V404 Cyg, its bolometric luminosity, averaged over an interval longer than the period of oscillation, spanned a wide range, from $\sim$0.01 $L_{\rm Edd}$ to $\sim$0.4 $L_{\rm Edd}$ (where $L_{\rm Edd}$ is the Eddington luminosity for a nine solar-mass black hole), as estimated from the hard X-ray flux and SED (Fig. 4 and Sec. 9 in Methods). Remarkably, the dip-type oscillations were observed at mean bolometric

luminosity of $\sim 0.015\ L_{\rm Edd}$, $\sim 0.07\ L_{\rm Edd}$, and $\sim 0.06\ L_{\rm Edd}$ during BJD 2,457,191.35–2,457,191.60, BJD 2,457,192.34–2,457,192.70, and BJD 2,457,200.60–2,457,200.76, respectively.

It is also worth noting that a typical dip similar to those seen in GRS 1915+105 was observed just 3 min after the first detection of this outburst (Extended Data Fig. 1b). These facts suggest that the accretion rate is not the critical parameter for inducing these oscillations. Our results imply that there is a novel type of disc instability different from the known dwarf-nova type[19] or Lightman-Eardley type[16] instability.

We point out that black hole binaries showing large-amplitude, short-term variations either in X-ray or optical bands have long orbital periods. (33.9 d in GRS 1915+105[20], $\sim$4 d in IGR J17091$-$3624[21], 6.5 d in V404 Cyg[22], and 2.8 d in V4641 Sgr[23]; Sec. 4 in Methods and Extended Data Table 3 for a comparison of these objects), reinforcing the earlier suggestion[24]. It has been proposed that the accretion disc in a system with a long orbital period suffers from instabilities in the vertical structure of the disc, and hence the disc beyond this radius of instability may never build up[15,25]. Our SED modeling of this outburst, however, requires a disc having a large radius ($\gtrsim 1.7 \times 10^{12}$ [cm]), even considering the uncertainty of the interstellar reddening, particularly to account for the ultraviolet flux. This result implies that the disc extended up to distances close to the maximum achievable radius (Sec. 8 in Methods). This radius is consistent with the short-term optical variations significantly detected below 0.01 Hz (Sec. 6 in Methods) and the time lag of $\sim$1 min between the X-ray and optical light curves (Fig. 3 and Extended Data Fig. 2) if we assume that the optical light mainly comes from reprocessed X-rays (Sec. 6 and Extended Data Fig. 5 in

Methods). We note that synchrotron emission has been proposed to be the origin of the short-term and large-amplitude fluctuations in case of V4641 Sgr[14]. The optical polarization of V404 Cyg, however, did not show evidence of significant variations during the 2015 outburst[26,27]. This fact disfavours synchrotron emission as the origin of the short-term variations.

Outbursts of X-ray transients are thought to be triggered by the dwarf-nova type instability: once the surface density at some radius reaches the critical density (Σ_{crit}) after continuous mass transfer from the secondary star, thermal instability occurs and the disc undergoes an outburst[19]. In systems with long orbital periods, it is difficult for surface densities in the outer disc to reach Σ_{crit}, which is roughly proportional to the radius[28]. As a result, thermal instability in the inner part of the disc occurs more easily and governs the outburst behaviour[29]. This is probably the reason why long-period systems behave differently than short-period "classical" X-ray transients. In fact, our estimate of the disc mass (5×10^{25} [g]) accreted during the 2015 outburst is far smaller than the mass (2×10^{28} [g]) of a fully built-up disc in quiescence (Sec. 5 in Methods and Extended Data Fig. 4). These values indicate that the surface density was well below the Σ_{crit} required to induce thermal instability in most parts of the disc at the onset of the present outburst. Once the X-ray outburst started in the inner region, hydrogen atoms in the outer part of the disc were ionized and "passively" maintained in the hot state as long as the X-ray illumination continued. This explains the large optical fluxes as observed[28]. The rapid decay observed in the 2015 outburst of V404 Cyg may reflect the lack of the exponential decay in long-period systems as theoretically predicted[30]. Because the surface densities in the rest of the disc were too low to sustain the outburst by viscous diffusion[19], only the inner part of the disc was responsible for the dynamics of the present outburst,

as inferred from the rapid fading from the outburst (Sec. 7 in Methods). We infer that, in outbursts of IGR J17091$-$3624[18,21] and the 1938 outburst of V404 Cyg (Sec. 5 and Extended Data Fig. 4 in Methods), the radius of the active disc is larger, which explains why the duration of those events is longer than that of the 2015 outburst of V404 Cyg.

1. Janiuk, A. & Czerny, B. On different types of instabilities in black hole accretion discs: implications for X-ray binaries and active galactic nuclei. *Mon. Not. R. Astron. Soc.* **414**, 2186–2194 (2011).

2. Fender, R. P. & Belloni, T. GRS 1915+105 and the disc-jet coupling in accreting black hole systems. *Annu. Rev. Astron. Astr.* **42**, 317–364 (2004).

3. Belloni, T., Klein-Wolt, M., Méndez, M., van der Klis, M. & van Paradijs, J. A model-independent analysis of the variability of GRS 1915+105. *Astron. Astrophys.* **355**, 271–290 (2000).

4. Hynes, R. I. *et al.* The remarkable rapid X-ray, ultraviolet, optical and infrared variability in the black hole XTE J1118+480. *Mon. Not. R. Astron. Soc.* **345**, 292–310 (2003).

5. Motch, C. & Ilovaisky, S. A. & Chevalier, C. Discovery of fast optical activity in the X-ray source GX 339$-$4. *Astron. Astrophys.* **109**, L1–L4 (1982).

6. Tanaka, Y. & Shibazaki, N. X-ray novae. *Annu. Rev. Astron. Astr.* **34**, 607–644 (1996).

7. Khargharia, J., Froning, C. S. & Robinson, E. L. Near-infrared spectroscopy of low-mass X-ray binaries: Accretion disk contamination and compact object mass determination in V404 Cyg and Cen X-4. *Astrophys. J.* **716**, 1105–1117 (2010).

8. Miller-Jones, J. C. A. *et al.* The first accurate parallax distance to a black hole. *Astrophys. J.* **706**, L230–L234 (2009).

9. Makino, F. GS 2023+338. *IAU Circ.* **4782** (1989).

10. Barthelmy, S. D. *et al.* Swift trigger 643949 is V404 Cyg. *GRB Coord. Netw. Circ.* **17929** (2015).

11. Negoro, H. *et al.* MAXI/GSC detection of a new outburst from the Galactic black hole candidate GS 2023+338 (V* V404 Cyg). *Astron. Telegram* **7646** (2015).

12. Chen, Y. T. *et al.* TAOS early optical observations of V404 Cyg. *Astron. Telegram* **7722** (2015).

13. Golenetskii, S. *et al.* Konus-Wind observation of Galactic transient V404 Cyg in outburst. *GRB Coord. Netw. Circ.* **17938** (2015).

14. Uemura, M. *et al.* Rapid optical fluctuations in the black hole binary V4641 Sagittarii. *Publ. Astron. Soc. Jpn.* **54**, L79–L82 (2002).

15. Życki, P. T., Done, C. & Smith, D. A. The 1989 May outburst of the soft X-ray transient GS 2023+338 (V404 Cyg). *Mon. Not. R. Astron. Soc.* **309**, 561–575 (1999).

16. Belloni, T., Méndez, M., King, A. R., van der Klis, M. & van Paradijs, J. An unstable central disk in the superluminal black hole X-ray binary GRS 1915+105. *Astrophys. J.* **479**, L145–L148 (1997).

17. Neilsen, J., Remillard, R. A. & Lee, J. C. The physics of the "heartbeat" state of GRS 1915+105. *Astrophys. J.* **737**, 69–108 (2011).

18. Altamirano, D. *et al.* The faint "heartbeats" of IGR J17091−3624: An exceptional black hole candidate. *Astrophys. J.* **742**, L17–L23 (2011).

19. Osaki, Y. Dwarf-nova outbursts. *Publ. Astron. Soc. Pac.* **108**, 39–60 (1996).

20. Steeghs, D. *et al.* The not-so-massive black hole in the microquasar GRS 1915+105. *Astrophys. J.* **768**, 185–191 (2013).

21. Janiuk, A., Grzedzielski, M., Capitanio, F. & Bianchi, S. Interplay between heartbeat oscillations and wind outflow in microquasar IGR J17091−3624. *Astron. Astrophys.* **574**, 92–102 (2015).

22. Casares, J., Charles, P. A. & Naylor, T. A 6.5-day periodicity in the recurrent nova V404 Cygni implying the presence of a black hole. *Nature* **355**, 614–617 (1992).

23. Orosz, J. A. *et al.* A black hole in the superluminal source SAX J1819.3−2525 (V4641 Sgr). *Astrophys. J.* **555**, 489–503 (2001).

24. Bagnoli, T. & in't Zand, J. J. M. Discovery of GRS 1915+105 variability patterns in the rapid burster. *Mon. Not. R. Astron. Soc.* **450**, L52–L56 (2015).

25. Hameury, J.-M., Menou, K., Dubus, G., Lasota, J.-P. & Hure, J.-M. Accretion disc outbursts: a new version of an old model. *Mon. Not. R. Astron. Soc.* **298**, 1048–1060 (1998).

26. Panopoulou, G., Reig, P. & Blinov, D. Optical polarization of V404 Cyg. *Astron. Telegram* **7674** (2015).

27. Itoh, R. *et al.* Optical and near-infrared polarimetry for V404 Cyg with 1.6m Pirka and 1.5m Kanata telescopes in Japan. *Astron. Telegram* **7709** (2015).

28. Lasota, J.-P. The disc instability model of dwarf novae and low-mass X-ray binary transients. *New. Astron. Rev.* **45**, 449–508 (2001).

29. Kim, S.-W., Wheeler, J. C. & Mineshige, S. Disk instability and outburst properties of the intermediate polar GK Persei. *Astrophys. J.* **384**, 269–283 (1992).

30. King, A. R. & Ritter, H. The light curves of soft X-ray transients. *Mon. Not. R. Astron. Soc.* **293**, L42–L48 (1998).

Author Contributions   M.K. led the campaign, performed optical data analysis and compiled all optical data. K.I. and A.I. performed optical data analysis. T.K., Y.U., D.N. and M.U. contributed to science discussions. S.N., M.S., T.E., T.H. and H.T. performed X-ray data analysis. Other authors than those mentioned above performed optical observations. M.K., K.I., T.K., Y.U., S.N., T.E., M.S., and A.I. wrote the manuscript. T.K., Y.U., and D.N. surpervised this project. M.K., K.I., T.K., Y.U., T.E., M.S., D.N., C.L., R.I., M.J.L., D.B.B., D.K., E.P.P., A.S.P., I.E.M., M.R., E.M., W.S., S.K., L.M.C., A.I., and M.U. improved the manuscript. All authors have read and approved the manuscript.

Author Information   Correspondence and requests for materials should be addressed to M.K. (mkimura@kusastro.kyoto-u.ac.jp).

Main figure legends:

Figure 1: Overall multi-colour light curves during the 2015 outburst of V404 Cyg.

This figure shows multi-colour light curves (B, V, R, I and no filters) during Barycentric Julian Day (BJD) 2,457,189–2,457,207 (BJD 2,457,189 corresponds to 2015 June 15). We can clearly see that dip-type oscillations (variations with recurrent sudden dips) were observed from beginning to end of the outburst. The horizontal axis represents BJD$-$2,457,189. The significant periods of repetitive optical variations are indicated in gray and green colours for the "dip-type" and "heartbeat-type" oscillations, respectively.

Figure 2: Short-term and large-amplitude optical variations having repeating structures in the 2015 outburst of V404 Cyg.

Panels a, b, c, and d represent variations with characteristic patterns during BJD 2,457,193.6–2,457,194.0, 2,457,197.7–2,457,198.0, 2,457,198.6–2,457,198.9, and 2,457,200.34–2,457,200.6, respectively. (a, b, and c) There are gradual rises with increasing amplitudes of fluctuations followed by dips, during which fluctuations disappear. These variations are sometimes accompanied with spikes. The interval between two dips is $\sim$45 min–$\sim$2.5 hours. (d) Repetitive small oscillations with high coherence are seen at intervals of $\sim$5 min. The shapes of these oscillations resemble those of GRS 1915+105[3].

Figure 3: Correlation between optical and X-ray fluctuations of V404 Cyg in the 2015 outburst.

The terms are (a) BJD 2,457,194.126–2,457,194.140, (b) 2,457,197.050–2,457,197.065,

16

(c) 2,457,198.760–2,457,198.780, and (d) 2,457,199.430–2,457,199.450, respectively. Panels a and b cover the fading and rising phases, respectively. Panels c and d show the correlations of short-term fluctuations. When both X-ray and optical light strongly varied, the correlation is generally good (though note in panels a, c, and d that optical dips lag behind X-ray dips). The navy blue error bars represent 1σ statistics errors. We plot points without errors when errors are sufficiently small.

Figure 4: The bolometric luminosity L_{bol} of V404 Cyg during the 2015 outburst.
It is normalized at the Eddington luminosity assuming a black hole mass of $9M_\odot$. The Swift/BAT survey data (15–50 keV) and INTEGRAL Imager on Board the Integral Satellite (IBIS)/CdTe array (ISGRI) monitoring (25–60 keV) are shown in black and red points, respectively. The gray and green markers represent the periods of the "dip-type oscillations" and "heartbeat-type oscillations", respectively. The black error bars represent 1σ statistical errors.

Methods

1 Detailed Methods of Optical Observations

Immediately after the detection by Swift/BAT on June 15.77197 UT, the VSNET collaboration team[31] started a worldwide photometric campaign of V404 Cyg. There was also an independent detection by CCD photometry on June 16.169 UT[32]. Time-resolved CCD photometry was carried out at 27 sites using 36 telescopes with apertures of dozens of centimetres (Extended Data Table 2). We also used the public AAVSO data[33]. We corrected for bias and flat-fielding in the usual manner, and performed standard aperture photometry. The observers except for TAOS[34] used standard filters (B, V, R_C, I_C; we write R and I for R_C and I_C in the main text and figures for brevity. (Extended Data Table 1) and measured magnitudes of V404 Cyg relative to local comparison stars whose magnitudes were measured by A. Henden (sequence 15167RN) from the AAVSO Variable Star Database[35]. We applied small zero-point corrections to some observers' measurements. When filtered observations were unavailable, we used unfiltered data to construct the light curve. The exposure times were mostly 2–30 s, with some exceptional cases of 120 s in B-band, giving typical time resolutions of a few seconds. All of the observation times were converted to Barycentric Julian Day.

2 Comparison with X-ray Observations

For the Swift/(XRT) light curves (Fig. 3 and Extended Data Fig. 2), we extracted source events from a region with a 30-pixel radius centered on V404 Cyg. To avoid pile-up effects, we further excluded an inner circular region if the maximum count rate of the XRT raw light curves, binned

18

in 10 s intervals, exceeded $200\,\mathrm{cts\,s^{-1}}$. The inner radii are set to be 10 and 20 pixels at the maximum raw rate of $1000\,\mathrm{cts\,s^{-1}}$ and $2000\,\mathrm{cts\,s^{-1}}$, respectively, and those for intermediate count rates were determined via linear interpolation between the two points. The presented light curves were corrected for the photon losses due to this exclusion by using the "xrtlccorr" tool. In addition, from panels a, c, and d of Fig. 3, we can see a time delay in the start of a dip in optical light, relative to that in X-rays. The delay time was ∼1 min, which is similar to the reported value of 0–50 s[36]. This was determined by cross-correlating the U-band and X-ray (0.3–10 keV) light curves obtained with Swift/UltraViolet and Optical Telescope (UVOT) and Swift/XRT on UT 2015 June 21[36]. The observations were carried out when the source showed little rapid optical flickering and no extreme flares, and thus the nature of the lag may be different from that in our observations. We also note that the apparent difference between the Swift/UVOT and the ground-based times[36] is caused by the drift of the clock on board on the satellite, to which we have applied the necessary corrections.

3 Origin of Cyclic Dips: X-ray Spectra Obtained with Swift/XRT during the Optical Observations

In order to examine the possibility that absorption by gas in the line-of-sight causes the observed violent flux variations in the optical and X-ray bands (Fig. 3), we studied intensity-sliced X-ray spectra. As a striking example, we show, in Extended Data Fig. 2a. This period corresponds to that in Fig. 3a when both the X-ray and optical fluxes exhibited a sudden intensity drop toward the latter part of the period. We divided it into five intervals (T1 to T5) (Extended Data Fig. 3a), and generated spectra through the tools "xrtpipeline" and "xrtproducts" for standard pipeline pro-

19

cessing. We excluded the central 60-arcsecond strip from this Windowed Timing (WT) mode data, to avoid the heavy pile-up effect when the raw count rate exceeds $\sim 150\,\mathrm{cts\,s^{-1}}$. We compared the νF_ν spectra of the five intervals, where the spectra are fitted by a single power-law model ("pegpwrlw") multiplied by photoelectric absorption ("phabs"). The absorbed X-ray flux ranges by two orders of magnitude from 2.1×10^{-9} erg s^{-1} cm^{-2} in T5 to 3.0×10^{-7} ergs s^{-1} cm^{-2} in T3. However, the best-fit column density and photon index were relatively stable over the five intervals, st $\sim 2 - 6 \times 10^{-21}$ cm^{-2} and $\sim$ 1.0–1.5, respectively. Since the X-ray spectrum does not show a noticeable rise in column density when the X-ray flux sharply dropped, and since there is no stronger iron edge in the latter part of the observation, absorption cannot be the primary cause of the time variation in our datasets that cover the X-ray and optical bands simultaneously.

4   Objects Showing Violent Short-term Variations in Outburst

We show the list of X-ray binaries which have shown violent short-term variations either in X-rays or in optical wavelengths (Extended Data Table 3).

IGR J17091−3624 is known as the second BH X-ray binary whose X-ray light curves showed a variety of patterns, resembling those of GRS 1915+105[18]. The variations classified as class ρ ("heartbeat"), class ν (similar to class ρ but with secondary peak after the dips), class α ("rounded-bumps"), class β/λ (repetitive short-term oscillations after low-quiet period), and class μ were observed in the 2011 outburst[18].

The Rapid Burster (RB or MXB 1730−335), a LMXB containing a neutron star (NS), was discovered by Small Astronomy Satellite (SAS-3) observations[37]. This object has been recently

20

reported to show cyclic long X-ray bursts with periods of a few seconds resembling class ρ variations ("heartbeat") in GRS 1915+105[24]. Another type of variations which are similar to class θ variations ("M"-shaped light curves) were also observed[24]. The emission of the Rapid Burster did not reach the Eddington luminosity during these variations[38].

V4641 Sgr was originally discovered as a variable star[39] and was long confused with a different variable star, GM Sgr[40]. The object is famous for its short and bright outburst in 1999, which reached a optical magnitude of at least 8.8 mag[41–44]. V4641 Sgr showed short-term variations in optical wavelengths during the 2002, 2003 and 2004 outbursts[14,45–47]. It was the first case in which short-term and large-amplitude variations in the optical range during an outburst were detected. V4641 Sgr is classified as a LMXB, and has a long orbital period. Its mass accretion rate is less than the Eddington rate (except for the 1999 outburst[44,48]). These properties are similar to those of V404 Cyg. However, while the short-term variations of V4641 Sgr seemed to be random, those of V404 Cyg showed repetitive patterns; this is the greatest difference between these two objects. There has been a suggestion that V4641 Sgr is a "microblazar"[49] because the jets observed during the outburst in 1999 were proposed to have the largest bulk Lorentz factor among known galactic sources[43].

There are also other X-ray transients showing short-term optical variations (e.g., XTE J1118+480 and GX 339−4). However, these two sources are Quasi-Periodic Oscillations (QPOs), characterized by very short periods. The periods are much shorter than those of repetitive patterns (tens of seconds to a few hours), which we discuss in this letter. Furthermore, the amplitudes of their variations are significantly smaller than those observed in V4641 Sgr[4,50] in timescales longer than

21

tens of seconds.

5   Estimation of the Disc Mass and Comparison with the Previous Outbursts

Following the method in [15], we estimated the mass stored in the disc at the onset of the outburst. By integrating the X-ray light curve of Swift/BAT and assuming the spectral model C in Table 1 in [15], we obtained 5.0×10^{25} [g] assuming a radiative efficiency of 10 per cent and a distance of 2.4 (± 0.2) kpc[8]. The mass during the 1989 outburst has been updated to 3.0×10^{25} [g] by using this updated distance. The stored mass in the 2015 outburst was approximately the same as that in the 1989 one. As discussed in [15], these masses are far smaller than the mass of a fully built-up disc, estimated to be 2.0×10^{28} [g], if these outbursts were starting at the outermost region.

We compare the published optical light curves of the 1989 and 1938 outbursts[51,52] with our data from the 2015 outburst (Extended Data Fig. 4). We can see that these outbursts have different durations. The 1938 outburst was apparently longer than the others, and it may have had different properties from the 1989 and 2015 ones. The fading rates of the 1989 and 2015 outbursts are significantly larger than those of classical X-ray transients[6], or FRED-type (fast rise and exponential decline) outbursts, such as 0.028 mag day^{-1} in V518 Per = GRO J0422+32[53] and 0.015 mag day^{-1} in V616 Mon = A0620$-$00[54]. This supports the hypothesis that the outbursts in 1989 and 2015 are different from typical outbursts of classical X-ray transients and that the stored disc mass was by a factor of $\sim 10^3$ smaller in the 1989 and 2015 outbursts than the mass of a fully built up disc.

6 Power Spectrum

We performed power spectral analyses on BJD 2,457,193, BJD 2,457,196, and BJD 2,457,200. We used the continuous and regularly sampled high-cadence dataset obtained by LCO (Extended Data Table 1) with exposure times of 5 s (on BJD 2,457,193) and 2 s (others). The durations of these observations are 1.4, 3.1 and 2.2 hours, respectively. Considering the read-out times of 1 s, the Nyquist frequencies of these observations are 0.08 and 0.17 Hz, respectively. The power spectral densities (PSDs) were calculated using "powspec" software in the FTOOLS Xronos package on magnitude measurements. We did not apply de-trending of the light curve since the durations of the individual observations were shorter than the timescale of the global variation of the outburst. The power spectra are well expressed by a power law [$P \propto f^{-\Gamma}$] with an index Γ of 1.9($\pm$ 0.1), 1.8($\pm$ 0.1), and 2.3($\pm$ 0.1) on BJD 2,457,193, 2,457,196, and 2,457,200, respectively (Extended Data Fig. 5). Interpretation of the physical origins based of these variations is difficult because a power law index of $\approx$2 in the PSDs is often observed in natural phenomena. In this region ($f <$ 0.01 Hz), the power originating in the optical variations of V404 Cyg is significantly higher than that of white noise estimated from the observations.

We next summarize the other reports on short-term variations of V404 Cyg during the present outburst. On BJD 2,457,191, this object was observed using the Argos photometer on the 2.1m Otto Struve Telescope at McDonald Observatory with an exposure time of 2 s[55]. They reported that the power spectrum was dominated by steep red noise. Observations on BJD 2,457,193 and BJD 2,457,194 were also performed using the ULTRACAM attached with the 4.2m William Herschel Telescope on La Palma observatory with a high time resolution (466.8 ms)[56]. They reported that

the variations were dominated by timescales longer than tens of seconds. Although large amplitude flares (0.3–0.4 mag) on time scales shorter than 1 s were reported[57], these flares may be of different origin. For the variations with timescales longer than 100 s, our results agree with these reports[55,56].

7 Disc Radius Inferred from Final Fading Rate

The timescale τ of heating/cooling waves in dwarf novae and X-ray transients[58] is a function of the central mass (M_1) and radius (r) with the form, $\tau \propto \alpha M_1^{-1/2} r^{3/2}$, where α is the viscosity parameter[59]. Here, we estimate the disc radius of V404 Cyg assuming that the timescale of the final fading reflected a dwarf nova-type cooling wave. Using the Kepler data of V344 Lyr[60] and V1504 Cyg, we measured a fading rate of 1.5 mag day^{-1} of the normal outbursts immediately preceding superoutbursts. During these outbursts, the disc radius is expected to be very close to the 3:1 resonance radius. Adopting a typical mass of a white dwarf in a cataclysmic variable ($M_1 = 0.83 M_\odot$[61]), we estimated the disc radius of V404 Cyg to be 7.8×10^{10} cm for a black hole mass of 9.0 $M_\odot$. This size is much smaller than the radius 1.2×10^{12} cm which is expected for a fully built-up disc[15].

8 Spectral Energy Distribution Modeling

Extended Data Fig. 6a shows the multi-wavelength spectral energy distribution on BJD 2,457,199.431–2,457,199.446, when the source was simultaneously observed in the X-ray, ultraviolet (UV), and optical bands. The optical fluxes in the V and I_C bands are taken from our photometric data averaged over the period. Note that R_C-band data are also available but not used here, because of the

contamination of the continuum strong Hα line[62–64].

The X-ray spectrum is extracted from simultaneous Swift/XRT data (ObsID 00031403058), which were taken in the Windowed Timing mode. The data are processed through the pipeline processing tool "xrtpipeline". The events detected within 20 pixels around the source position are removed to mitigate pileup effects. The U-band flux is obtained from the Swift/UVOT images with the same ObsID as the XRT, through the standard tool "uvot2pha" provided by the Swift team. A circular region centred at the source position with a radius of 5 arcsec is adopted as the source extraction region of the UVOT data. The optical, UV, and X-ray data are corrected for interstellar extinction/absorption by assuming $A_{\rm V} = 4$[65] and using the extinction curve in [66] and the $N_{\rm H}$ versus $E(B - V)$ relation in [67]. Radio data are from the RATAN-600 observation performed in the same period[68].

The multi-wavelength SED can be reproduced with the "diskir" model[69,70], which accounts for the emission from the accretion disc, including the effects of Comptonisation in the inner disc and reprocessing in the outer disc. We find that partial covering X-ray absorption (using the "pcfabs" model implemented in the spectral analysis software XSPEC) improves the quality of the fit significantly. The inner disc temperature is estimated to be 0.12 ± 0.01 keV, and the electron temperature and photon index of the Comptonisation component, the ratio between the luminosity of the Compton tail and disc blackbody ($L_{\rm C}/L_{\rm d}$), and the fraction of the bolometric flux thermalized in the outer disc ($f_{\rm out}$), are 17.5 ± 0.8 keV, 1.78 ± 0.03, 1.17 ± 0.03, and $1.3^{+0.6}_{-0.8} \times 10^{-2}$, respectively (the errors in this section represent 90% confidence ranges for one parameter). The inner radius ($R_{\rm in}$) is estimated to be $(1.5 - 5.4) \times 10^8$ cm, and the outer radius ($R_{\rm out}$) is $(2.5 \pm$

$0.3) \times 10^{12}$ cm. The derived value of R_{out} is comparable to or even larger than the binary separation ($\sim 2.2 \times 10^{12}$ cm). However, it can be smaller due to uncertainties in interstellar/circumbinary extinction[71] and/or the contribution of jet emission. For instance, if A_V is 0.4 magnitude larger than the assumed value (4.0), R_{out} becomes $1.9 \pm 0.2 \times 10^{12}$ cm. The maximum achievable radius of a stable disc for a q (mass ratio) = 0.06 object (Extended Data Table 3) is around $0.62A$ (radius of the 2:1 resonance) to $\sim 0.7A$ (tidal limit), where A is the binary separation[72]. Considering the uncertainties, the result of our analysis ($\gtrsim 0.77A$) is compatible with this maximum radius. Our result appears to favour a large A_V value. For the partial covering absorber, the best-fit value of the column density is $5.2^{+0.4}_{-0.5} \times 10^{23}$ cm^{-2} and that of the covering fraction is $64 \pm 4\%$.

The radio SED can be approximated by a power-law with a photon index of ≈ 1, as in other black hole binaries in the low/hard state[73]. This profile is likely generated by the optically-thick synchrotron emission from compact jets[74]. Because optically-thick synchrotron spectrum often extends up to the mm to near-infrared bands[75–77], it may contribute to the optical fluxes, in particular at longer wavelengths. The blackbody emission from the companion, a K3III-type star[7] with a radius of ~ 3 $R_\odot$ and a temperature of ~ 4320 K, contributes to the SED only negligibly.

Extended Data Fig. 6b plots the simultaneous SED on BJD 2,457,191.519–2,457,191.524, which is ~ 2 orders of magnitude fainter in the X-ray band than that shown in the left panel. The X-ray, UV, and optical data are taken from the Swift data (ObsID 00031403038) and our photometric measurements in same manner as described above. This SED can be reproduced with the irradiated disc model as well, with somewhat smaller photon index ($1.43^{+0.02}_{-0.03}$) and inner disc temperature (< 0.07 keV), and a larger f_{out} ($0.06^{+0.02}_{-0.05}$) than those on BJD 2,457,199.431–2,457,199.446.

9 Time History of the Bolometric Luminosity

The bolometric luminosity L_{bol} of V404 Cyg is evaluated based on the hard X-rays above $\sim$15 keV where the intrinsic spectrum is less affected by an absorption.

We processed the Swift/BAT archival survey data via "batsurvey" in the HEAsoft package to derive count rates with individual exposures of $\sim$300 seconds. Even within this short exposure, photon statistics are good during bright states (>0.05 counts s^{-1}). Assuming a Crab-like spectrum (1 Crab$\sim$ 0.039 counts s^{-1}), the BAT count rates R (counts s^{-1}) are then converted into 15–50 keV flux (F_{15-50}) and luminosity (L_{15-50}) using $F_{15-50} = 3.6 \times 10^{-7} R$ (erg s^{-1} cm^{-1}) and a fiducial distance of 2.4 kpc, respectively. In Fig. 4, we show L_{bol} after multiplying by a conversion factor $L_{bol}/L_{15-50} = 7$ determined from SED modelling (Sec. 8 in Methods). We find that this bolometric correction factor lies within the range of 2.5–10 by fitting nineteen X-ray(XRT)-optical simultaneous SED in different periods between BJD 2,457,192.019 and 2,457,201.011. Since the BAT survey data are rather sparse, in order to catch shorter-term variations, we further overlaid the INTEGRAL IBIS/ISGRI monitoring in the 25–60 keV band available at[78], assuming a conversion parameter of 1 Crab rate to be 172.1 counts s^{-1} and a bolometric correction factor at 9.97.

The luminosity was highly variable during the outburst, changing by five orders of magnitude. While V404 Cyg sometimes reaches the Eddington luminosity (L_{Edd}) at the peak of multiple sporadic flares, it also repeatedly dropped below 1–10% of L_{Edd} (Fig. 4). At earlier phases of this outburst, the characteristic oscillation already occurred during a lower luminosity state as discussed in the main text.

31. Kato, T. *et al.* Variable Star Network: World center for transient object astronomy and variable stars. *Publ. Astron. Soc. Jpn.* **56**, S1–S54 (2004).

32. Muyllaert, E. *BAAVSS (The British Astronomical Association Variable Star Section) alert* **4101** (2015). https://groups.yahoo.com/neo/groups/baavss-alert/conversations/messages/4101.

33. http://www.aavso.org/data-download/.

34. Lehner, M. J. *et al.* The Taiwanese-American Occultation Survey: The multi-telescope robotic observatory. *Publ. Astron. Soc. Pac.* **121**, 138–152 (2009).

35. http://www.aavso.org/vsp.

36. Gandhi, P. *et al.* Correlated optical and X-ray variability in V404 Cyg. *Astron. Telegram* **7727** (2015).

37. Lewin, W. H. G. *et al.* The discovery of rapidly repetitive X-ray bursts from a new source in Scorpius. *Astrophys. J.* **207**, L95–L99 (1976).

38. Bagnoli, T., in't Zand, J. J. M., Galloway, D. K. & Watts, A. L. Indications for a slow rotator in the Rapid Burster from its thermonuclear bursting behaviour. *Mon. Not. R. Astron. Soc.* **431**, 1947–1955 (2013).

39. Goranskij, V. P. Variable stars in Sagittarius. *Astron. Tsirk.* **1024**, 3–4 (1978).

40. Samus, N. N. *et al.* V4641 Sagittarii and GM Sagittarii. *IAU Circ.* **7277** (1999).

41. Stubbings, R. *et al.* GM Sagittarii and SAX J1819.3−2525 = XTE J1819−254. *IAU Circ.* **7253** (1999).

42. Kato, T., Uemura, M., Stubbings, R., Watanabe, T. & Monard, B. Preoutburst activity of V4641 Sgr = SAX J1819.3−2525: Possible existence of 2.5-day period. *Information Bull. on Variable Stars* **4777** (1999).

43. Hjellming, R. M. *et al.* Light curves and radio structure of the 1999 september transient event in V4641 Sagittarii (=XTE J1819−254 = SAX J1819.3−2525). *Astrophys. J.* **544**, 977–992 (2000).

44. Uemura, M. *et al.* The 1999 optical outburst of the fast X-ray nova, V4641 Sagittarii. *Publ. Astron. Soc. Jpn.* **54**, 95–101 (2002).

45. Uemura, M. *et al.* Outburst and post-outburst active phase of the black hole X-ray binary, V4641 Sgr in 2002. *Publ. Astron. Soc. Jpn.* **56**, S61–S75 (2004).

46. Uemura, M. *et al.* Optical observation of the 2003 outburst of a black hole X-ray binary, V4641 Sagittarii. *Publ. Astron. Soc. Jpn.* **56**, 823–829 (2004).

47. Uemura, M. *et al.* Outburst of a black hole X-ray binary V4641 Sgr in 2004 July. *Information Bull. on Variable Stars* **5626**, 1–4 (2005).

48. Revnivtsev, M., Sunyaev, R., Gilfanov, M. & Churazov, E. V4641 Sgr - a super-eddington source enshrouded by an extended envelope. *Astron. Astrophys.* **385**, 904–908 (2002).

49. Mirabel, I. F. & Rodríguez, L. F. Sources of relativistic jets in the Galaxy. *Annu. Rev. Astron. Astr.* **37**, 409–443 (1999).

50. Imamura, J. N., Kristian, J., Middleditch, J. & Steiman-Cameron, T. Y. The 8 second optical quasi-periodic oscillations in GX 339−4. *Astron. Astrophys.* **365**, 312-316 (1990).

51. Casares, J., Charles, P. A., Jones, D. H. P., Rutten, R. G. M. & Callanan, P. J. Optical studies of V404 Cyg, the X-ray transient GS 2023+338. I – the 1989 outburst and decline. *Mon. Not. R. Astron. Soc.* **250**, 712–725 (1991).

52. Wagner, R. M. *et al.* Optical identification of the X-ray source GS 2023+338 as V404 Cygni. *Astrophys. J.* **378**, 293–297 (1991).

53. Chevalier, C. & Ilovaisky, S. A. CCD photometry of GRO J0422+32 during activity and quiescence. *Astron. Astrophys.* **297**, 103–114 (1995).

54. Whelan, J. A. J. *et al.* Spectroscopic observations of the X-ray nova A0620−00. *Mon. Not. R. Astron. Soc.* **180**, 657–673 (1977).

55. Hynes, R. I., Robinson, E. L. & Morales, J. Rapid optical photometry of V404 Cyg. *Astron. Telegram* **7677** (2015).

56. Gandhi, P. *et al.* Sub-second multi-band optical timing of V404 Cyg with ULTRACAM. *Astron. Telegram* **7686** (2015).

57. Hynes, R. I., Robinson, E. L. & Morales, J. Further rapid optical photometry of V404 Cyg. *Astron. Telegram* **7710** (2015).

58. Cannizzo, J. K. On the relative rates of decay of the optical and soft X-ray fluxes in dwarf nova outbursts. *Astrophys. J.* **473**, L41–L44 (1996).

59. Meyer, F. Transition waves in accretion disks. *Astron. Astrophys.* **131**, 303–308 (1984).

60. Cannizzo, J. K., Smale, A. P., Wood, M. A., Still, M. D. & Howell, S. B. The Kepler light curves of V1504 Cygni and V344 Lyrae: A study of the outburst properties. *Astrophys. J.* **747**, 117–128 (2012).

61. Savoury, C. D. J. *et al.* Cataclysmic variables below the period gap: mass determinations of 14 eclipsing systems. *Mon. Not. R. Astron. Soc.* **415**, 2025–2041 (2011).

62. Munoz-Darias, T., Sanchez, D. M. & Casares, J. Optical spectroscopy of V404 Cyg: evolution of the P Cygni profiles. *Astron. Telegram* **7669** (2015).

63. Caballero-Garcia, M. D., Castro-Tirado, A. J., Oates, S. & Jeong, S. Early optical spectroscopy follow-up of V404 Cyg with GTC/OSIRIS. *Astron. Telegram* **7699** (2015).

64. Scarpaci, J., Maitra, D., Hynes, R. & Markoff, S. Multi-band optical observations of V404 Cygni and correlated spectral changes. *Astron. Telegram* **7737** (2015).

65. Casares, J., Charles, P. A., Naylor, T. & Pavlenko, E. P. Optical studies of V404 Cygni the X-ray transient GS 2023+338 – part three – the secondary star and accretion disc. *Mon. Not. R. Astron. Soc.* **265**, 834–852 (1993).

66. Cardelli, J. A., Clayton, G. C. & Mathis, J. S. The relationship between infrared, optical, and ultraviolet extinction. *Astrophys. J.* **345**, 245–256 (1989).

67. Bohlin, R. C., Savage, B. D. & Drake, J. F. A survey of interstellar H I from Lα absorption measurements. II. *Astrophys. J.* **224**, 132–142 (1978).

68. Trushkin, S. A., Nizhelskij, N. A. & Tybulev, P. G. The inverted radio spectrum of the flare in V404 Cyg. *Astron. Telegram* **7667** (2015).

69. Gies, D. R. *et al.* Stellar wind variations during the X-ray high and low states of Cygnus X-1. *Astrophys. J.* **678**, 1237–1247 (2008).

70. Kaptein, R. G. *et al.* Discovery of 1RXS J171824.2−402934 as an X-ray burster. *Astron. Astrophys.* **358**, L71–L74 (2000).

71. Hynes, R. I. *et al.* The quiescent spectral energy distribution of V404 Cyg. *Mon. Not. R. Astron. Soc.* **399**, 2239–2248 (2009).

72. Osaki, Y. & Meyer, F. Early humps in WZ Sge stars. *Astron. Astrophys.* **383**, 574–579 (2002).

73. Fender, R. P. Powerful jets from black hole X-ray binaries in low/hard X-ray states. *Mon. Not. R. Astron. Soc.* **322**, 31–42 (2001).

74. Blandford, R. D. & Königl, A. Relativistic jets as compact radio sources. *Astrophys. J.* **232**, 34–48 (1979).

75. Corbel, S. & Fender, R. P. Near-infrared synchrotron emission from the compact jet of GX 339−4. *Astrophys. J.* **573**, L35–L39 (2002).

76. Gandhi, P. *et al.* A variable mid-infrared synchrotron break associated with the compact jet in GX 339−4. *Astrophys. J.* **740**, L13–L19 (2011).

77. Russell, T. D. *et al.* The accretion-ejection coupling in the black hole candidate X-ray binary MAXI J1836−194. *Mon. Not. R. Astron. Soc.* **439**, 1390–1402 (2014).

78. http://www.isdc.unige.ch/integral/analysis#QLAsources.

79. Kloppenborg, B. K., Pieri, R., Eggenstein, H.-B., Maravelias, G. & Pearson, T. A demonstration of accurate wide-field V-band photometry using a consumer-grade DSLR camera. *J. American Assoc. Variable Star Obs.* **40**, 815–833 (2012).

80. Wang, J. H. *et al.* Early optical brightening in GRB 071010B. *Astrophys. J.* **679**, L5–L8 (2008).

81. Alcock, C. *et al.* TAOS: The Taiwanese-American Occultation Survey. *Earth Moon and Planets* **92**, 459–464 (2003).

82. Zhang, Z.-W. *et al.* The TAOS project: Results from seven years of survey data. *Astron.J.* **146**, 14–23 (2013).

83. Casares, J. & Charles, P. A. Optical studies of V404 Cyg, the X-ray transient GS 2023+338. IV. the rotation speed of the companion star. *Mon. Not. R. Astron. Soc.* **271**, L5–L9 (1994).

84. Wijnands, R., Yang, Y. J. & Altamirano, D. The enigmatic black hole candidate and X-ray transient IGR J17091−3624 in its quiescent state as seen with XMM-Newton. *Mon. Not. R. Astron. Soc.* **422**, L91–L95 (2012).

85. Reid, M. J. *et al.* A parallax distance to the microquasar GRS 1915+105 and a revised estimate of its black hole mass. *Astrophys. J.* **796**, 2–9 (2014).

86. Iyer, N., Nandi, A. & Mandal, S. Determination of the mass of IGR J17091−3624 from "spectro-temporal" variations during the onset phase of the 2011 outburst. *Astrophys. J.* **807**, 108-116 (2015).

87. Sala, G. *et al.* Constraints on the mass and radius of the accreting neutron star in the Rapid Burster. *Astrophys. J.* **752**, 158–164 (2012).

88. MacDonald, R. K. D. *et al.* The black hole binary V4641 Sagitarii: Activity in quiescence and improved mass determinations. *Astrophys. J.* **784**, 2–20 (2014).

89. Fender, R. P. *et al.* MERLIN observations of relativistic ejections from GRS 1915+105. *Mon. Not. R. Astron. Soc.* **304**, 865-874 (2014).

90. King, A. L. *et al.* An extreme X-ray disk wind in the black hole candidate IGR J17091−3624. *Astrophys. J.* **746**, L20–L24 (2012).

91. Szkody, P. *et al.* V404 Cygni. *IAU Circ.* **4794** (1989).

Legends for the Extended Data tables:

Extended Data Table 1: A log of photometric observations of the 2015 outburst of V404 Cyg. Start and end dates of observations, mean magnitudes, 1σ of mean magnitudes, numbers of observations, observers' codes, and filters are summarized. Note that observers for TAOS used custom made filters close to the union of standard R and V[34], but the magnitude reported in this paper was approximately calibrated to standard R.

Extended Data Table 2: List of instruments for optical observations. Observers' codes (CODE) (see Extended Data Table 1), names of telescopes & CCD cameras, observatory (or observer) and sites are summarized.

Extended Data Table 3: Basic information on objects showing violent short-term variations in outbursts. Orbital period, nature of the compact object, spectrum of the secondary, mass of the central object (M_1), mass ratio (q), inclination angle (i), minimum magnitude (V-band), and maximum magnitude (V-band) on V404 Cyg, GRS 1915+105, IGR 17091−3624, the Rapid Burster, and V4641 Sgr.

Legends for the Extended Data figures:

Extended Data Fig. 1: Optical and X-ray light curves of V404 Cyg during an outburst in 2015 June–July.

Panel a shows overall multi-colour light curves and Swift/BAT light curves. The plotted points are averaged for every 0.67 days. Panel b is an enlarged view of the shaded box in panel a (the first detection of short-term variations). On BJD 2,457,203, the mean magnitude dropped below V=17.0. Superimposed on this rapid fading, the amplitude of variations became progressively smaller and smaller. After BJD 2,457,205, the mean magnitude seemed to be constant, and the outburst virtually ended. The term"mag" is the abbreviation for magnitude.

Extended Data Fig. 2: Additional examples of simultaneous optical and X-ray observations of V404 Cyg in the 2015 outburst except those in Fig. 3.

The left panels of panels a and b represent the correlations on BJD 2,457,192 and BJD 2,457,200, respectively. In the right panels, Swift/XRT light curves in linear scales are shown. The navy blue error bars represent 1σ statistic errors.

Extended Data Fig. 3: Example of the soft X-ray light curve and spectra during the dip-type oscillation in the 2015 outburst of V404 Cyg.

(a) The $\sim$860 s-long Swift/XRT raw light curve (BJD 2,457,194.125–2,457,194.135, ObsID 00031403040) without pile-up correction, same as the X-ray data in Fig. 3a of the main paper. (b) Time-sliced soft X-ray spectra with pile-up correction, in the intervals of T1 to T5 determined in panel a. The exposures of individual spectra are $\sim$100–300 sec. The error bars

36

represent 1σ statistics errors.

Extended Data Fig. 4: Comparison of the 1938, 1989 and 2015 outbursts of V404 Cyg.

The horizontal axis represents days BJD$-2{,}429{,}186$, BJD$-2{,}447{,}673$, and BJD$-2{,}457{,}189$, respectively. Photographic magnitudes are approximately the same as B-band.

Extended Data Fig. 5: Power spectral densities of the early stage, the middle stage, and the later stage in the 2015 outburst of V404 Cyg.

Power spectral densities of the fluctuations on BJD 2,457,193 (top, circles), BJD 2,457,196 (middle, triangles), and BJD 2,457,200 (bottom, rectangles). The abscissa and ordinate denote the frequency in Hz units and the power in arbitrary units, respectively. For better visualization, the obtained spectrum is multiplied by 8×10^{-4} on BJD 2,457,196 and by 10^{-4} on BJD 2,457,200. The errors are 1σ-corresponding values obtained from relevant chi-square distributions of the power spectra.

Extended Data Fig. 6: Simultaneous, extinction-corrected multi-wavelength SEDs of V404 Cyg.

The intervals shown are (a) BJD 2,457,199.431–2,457,199.446 and (b) BJD 2,457,191.519–2,457,191.524. The optical (V and $I_{\rm C}$) fluxes are averaged over the intervals, and the error bars represent their standard errors. The X-ray, U and $UW2$-band data are obtained with Swift and the errors represent 1σ statistic errors. The radio fluxes (open squares) are compiled from the RATAN-600 results at BJD 2,457,199.433[68]. The red solid and dotted lines show the contribution of emissions from the irradiated disc with Comptonisation and from the companion star, respectively. The blue dashed

line approximates the radio SED, which is extended to the optical bands for illustrative purposes.

Figure 1
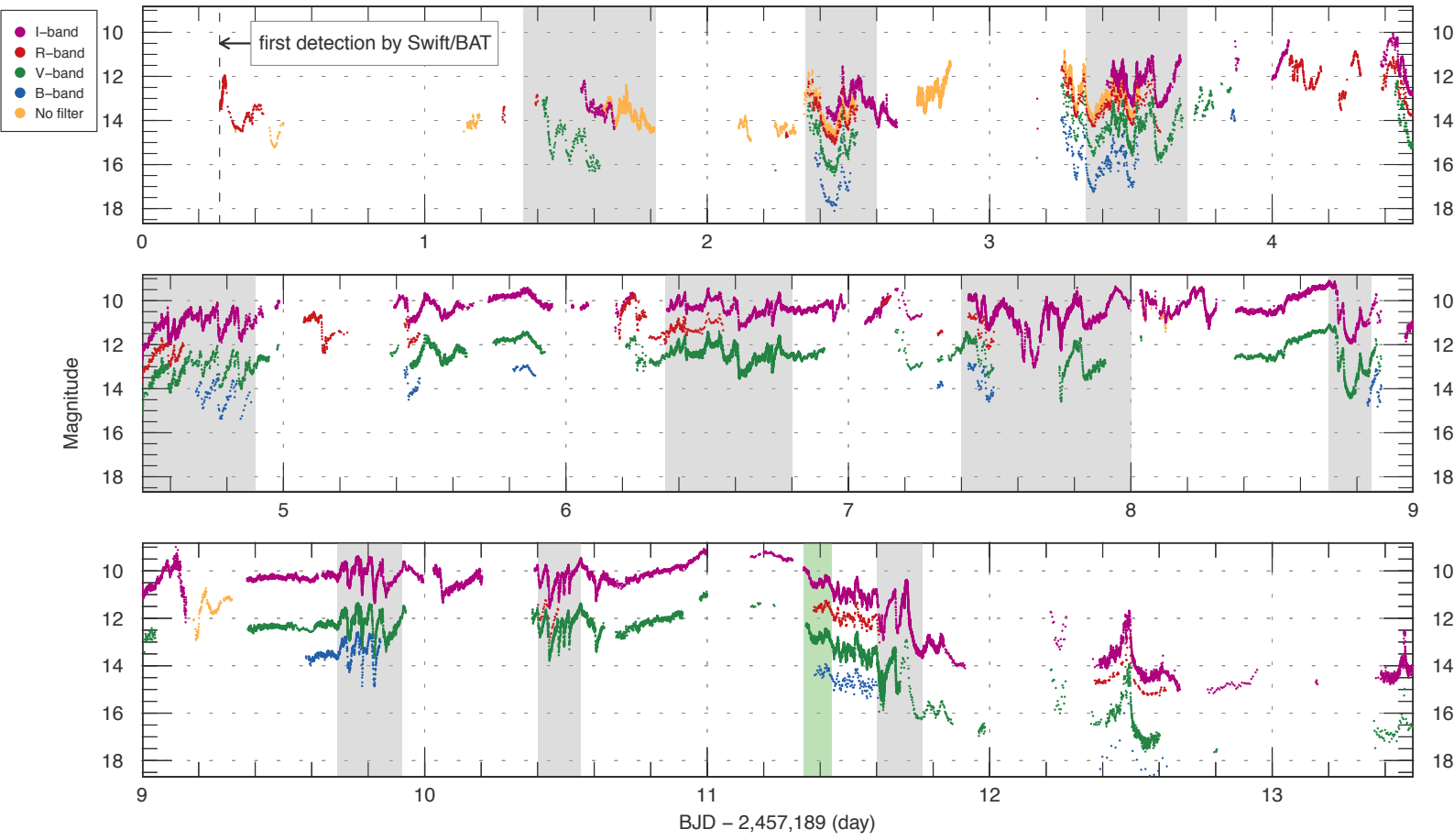
Figure 2

Figure 3

Figure 4

a

Legend:
- I-band − 3 mag
- R-band
- V-band + 3 mag
- B-band + 6 mag
- Swift/BAT 15–50 keV × 10^6 counts
- Swift/BAT 50–150 keV × 10^4 counts

(b)

Magnitude

BJD−2,457,189 (day)

Extended Data Fig. 1

b

Magnitude

1 hour

first detection by Swift/BAT

- R-band
- No filter

BJD−2,457,189 (day)
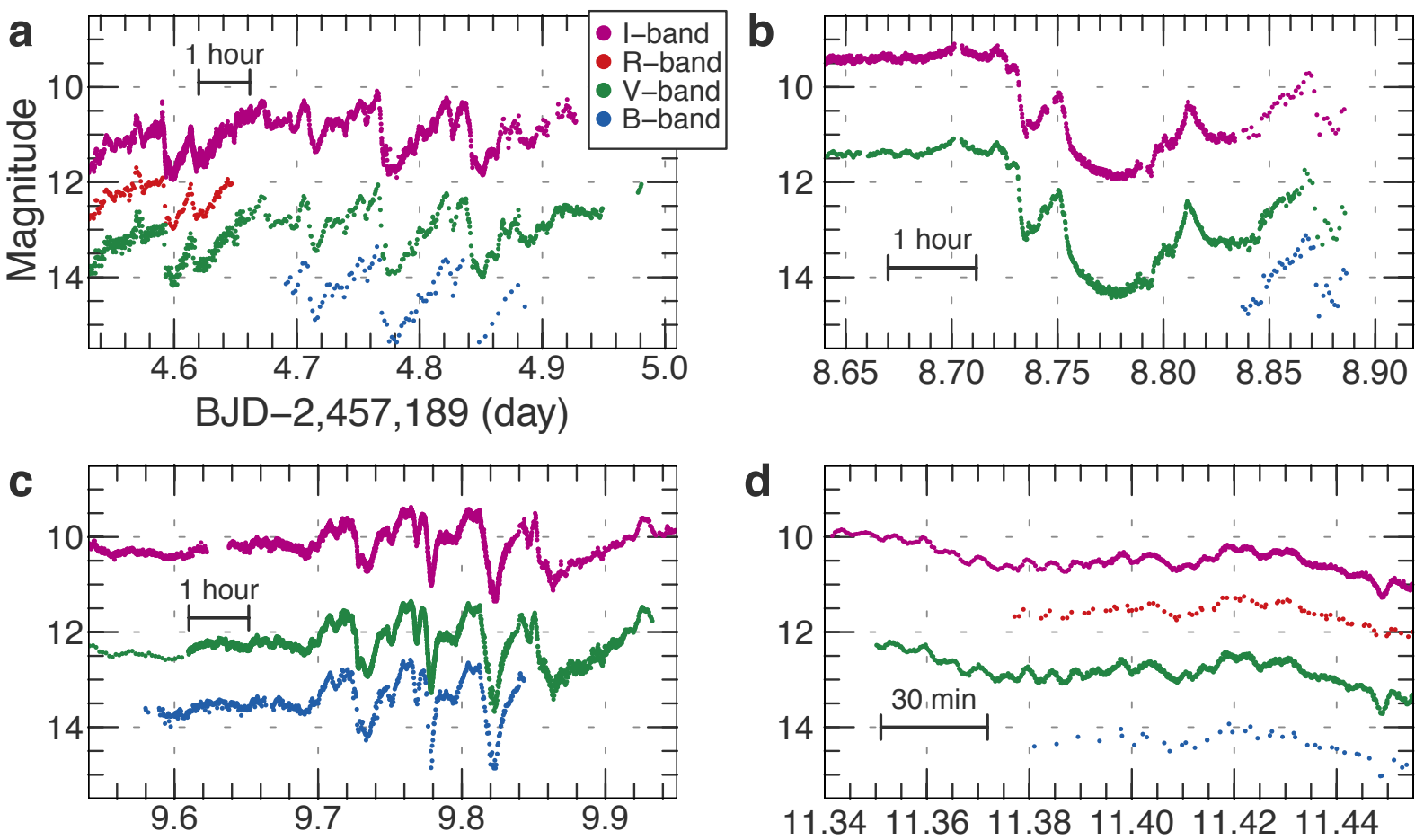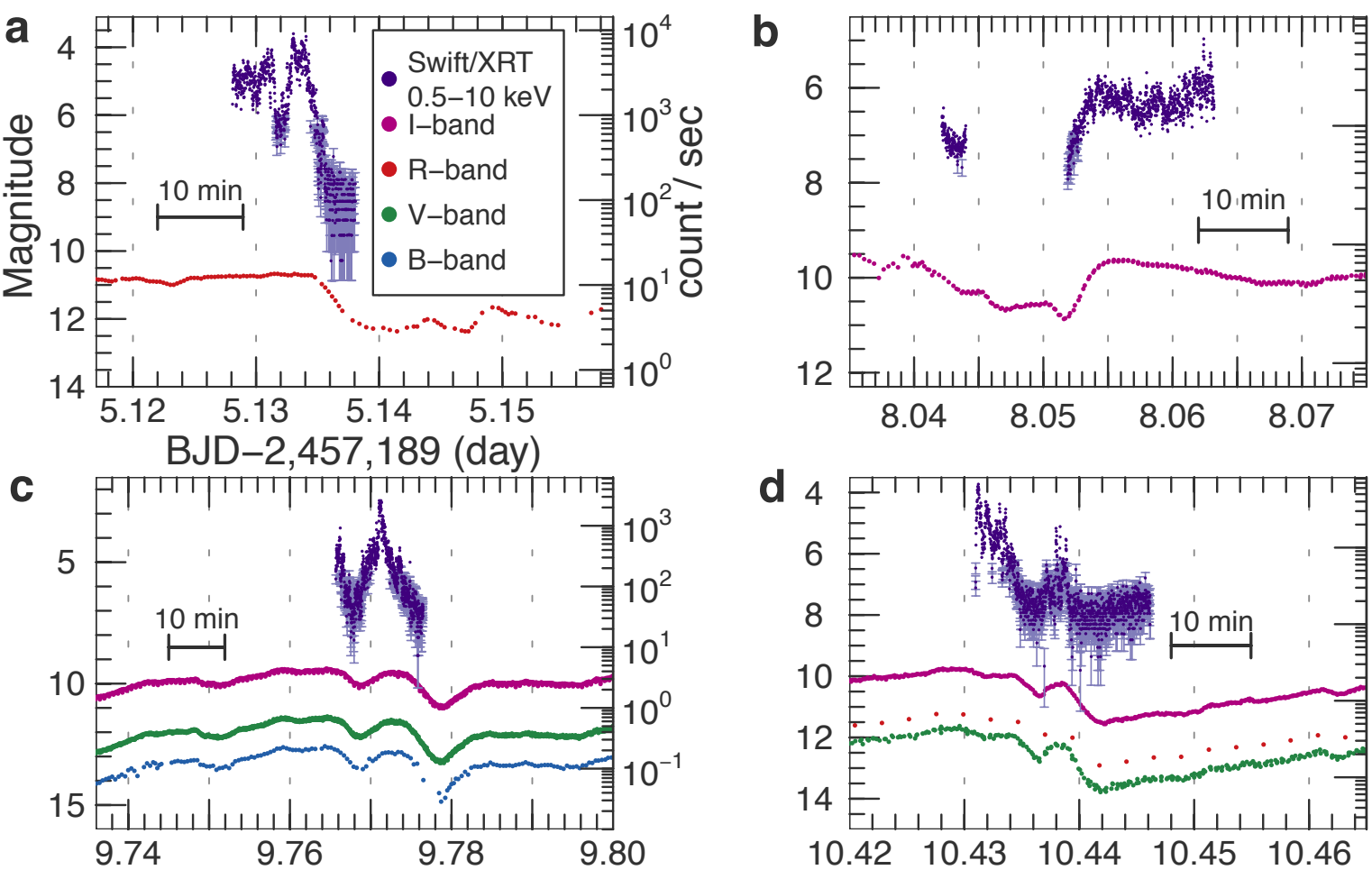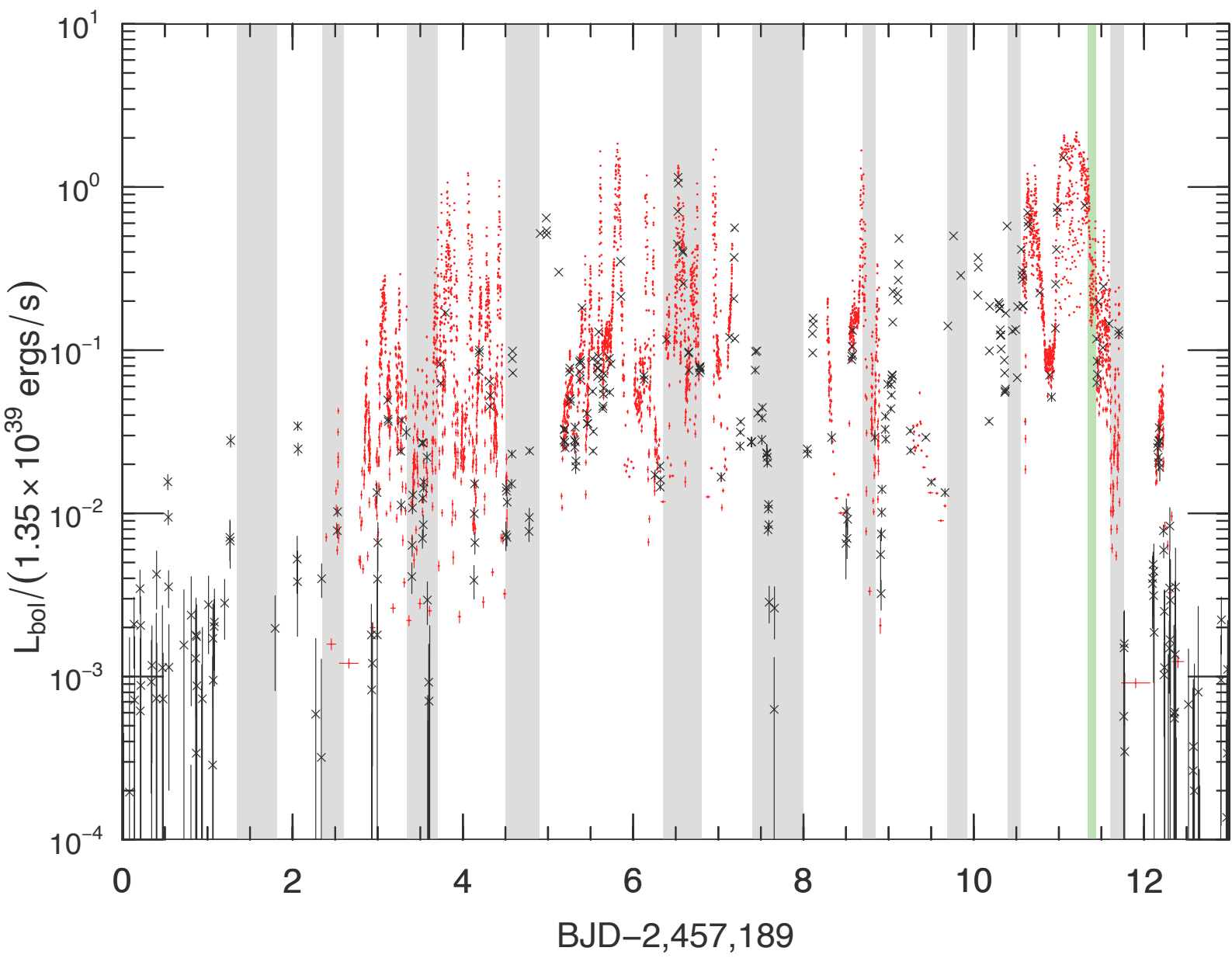
Extended Data Fig. 2

Extended Data Fig. 3

Extended Data Fig. 4

Extended Data Fig. 5

a

keV² (Photons cm⁻² s⁻¹ keV⁻¹)

keV^2 (Photons cm^{-2} s^{-1} keV^{-1})

radio
(RATAN-600)

I$_C$ V U

X-ray
(Swift)

Energy (keV)

b

keV^2 (Photons cm^{-2} s^{-1} keV^{-1})

I$_C$ V UW2

X-ray
(Swift)

Energy (keV)
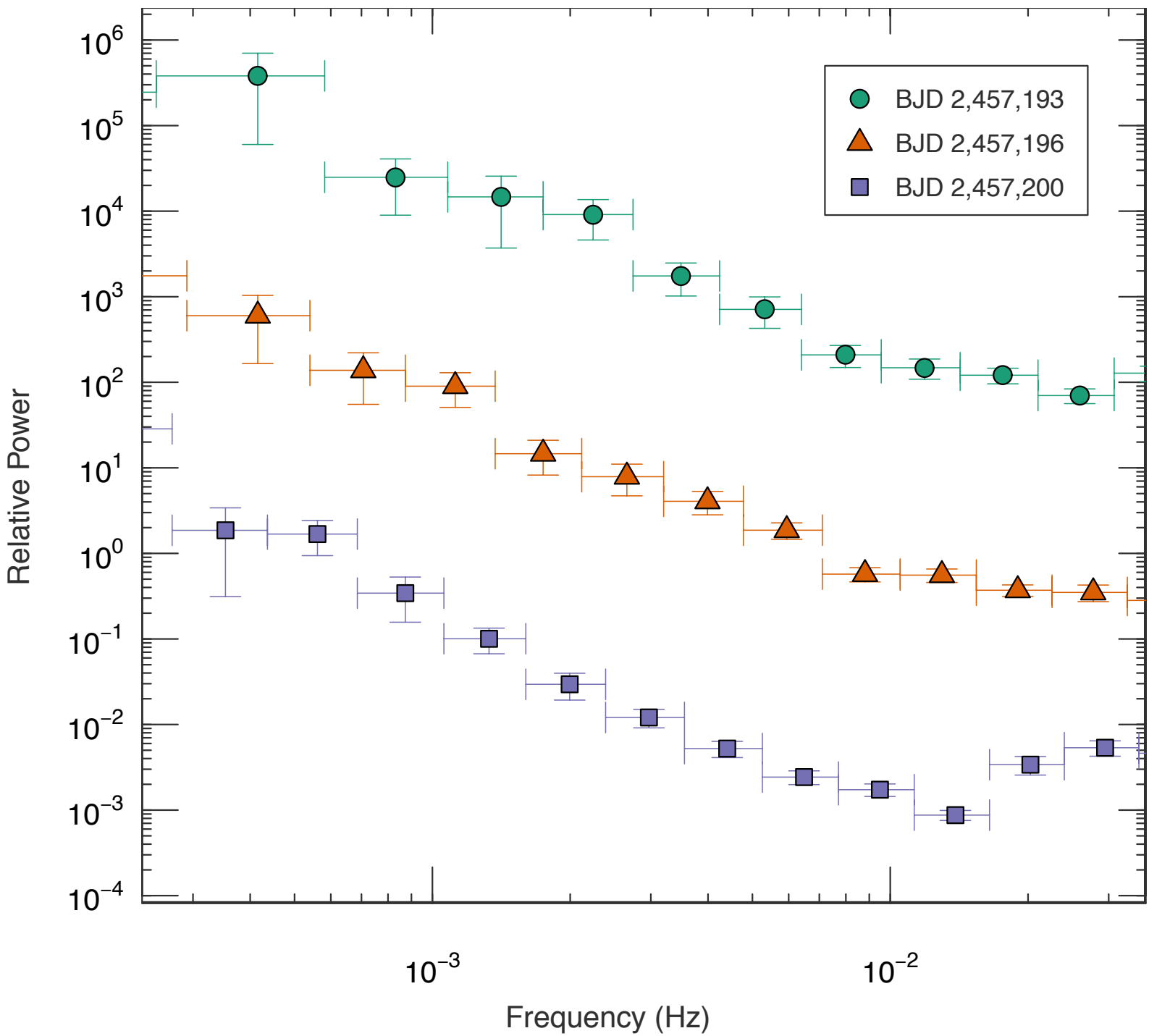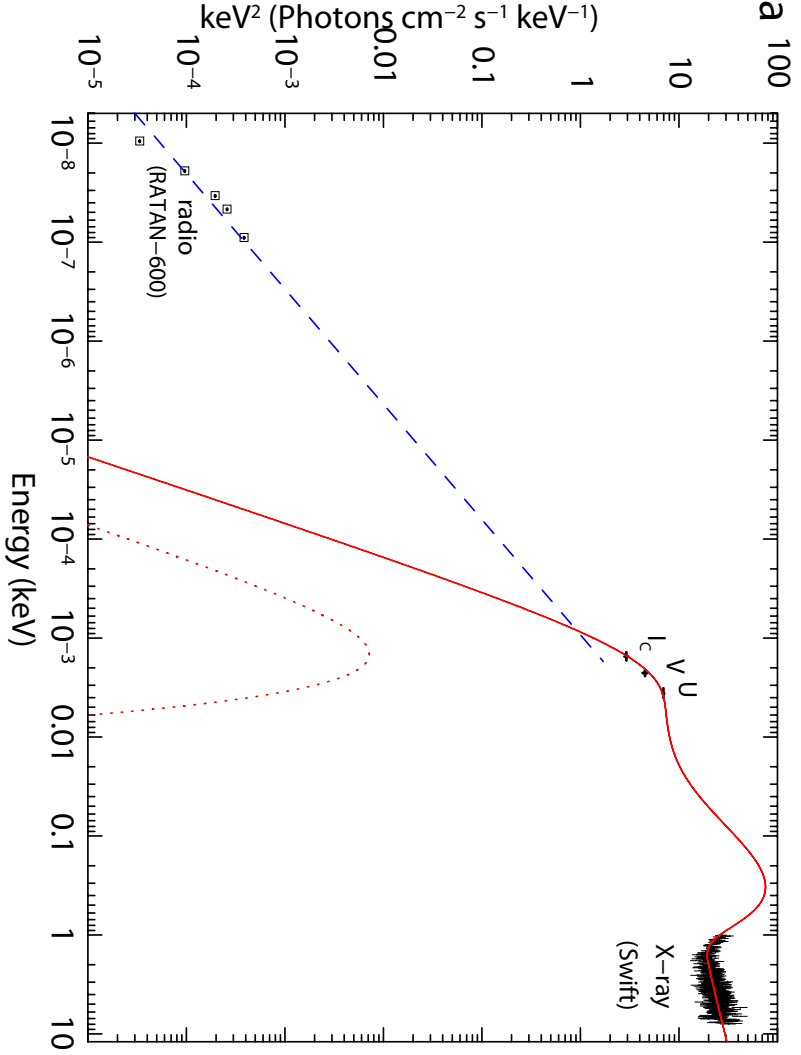
Extended Data Fig. 6

Extended Data Table 1

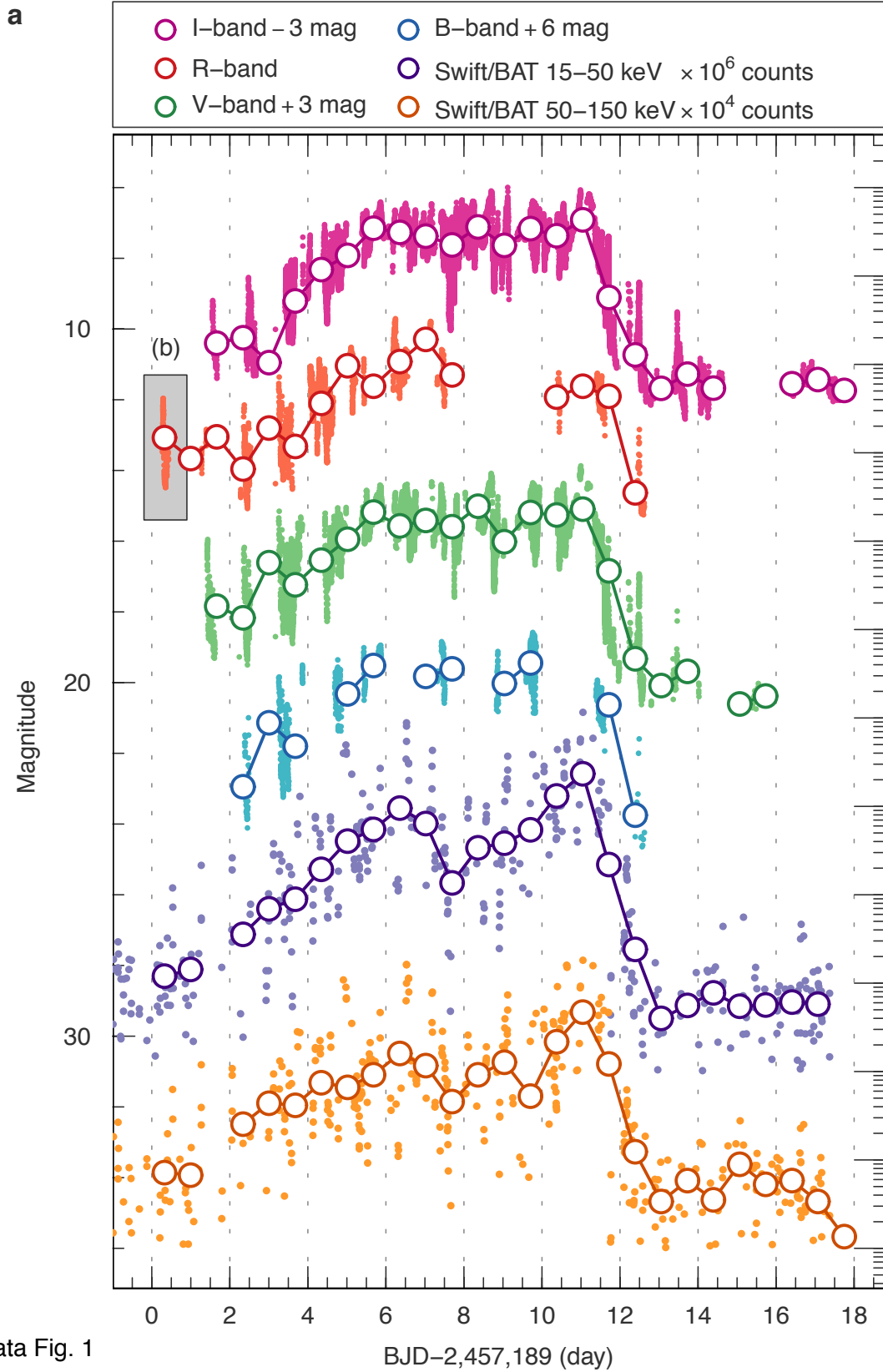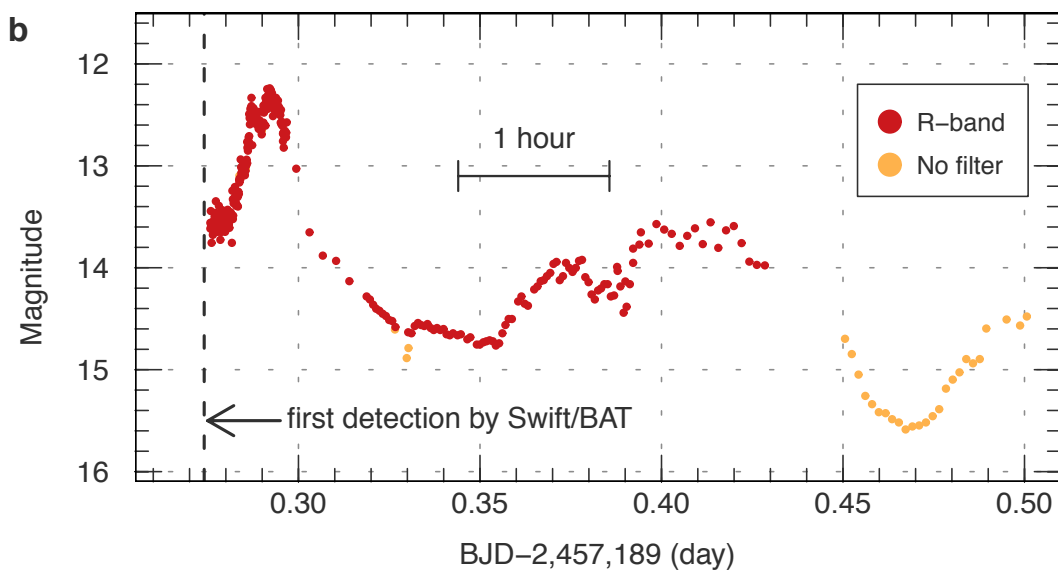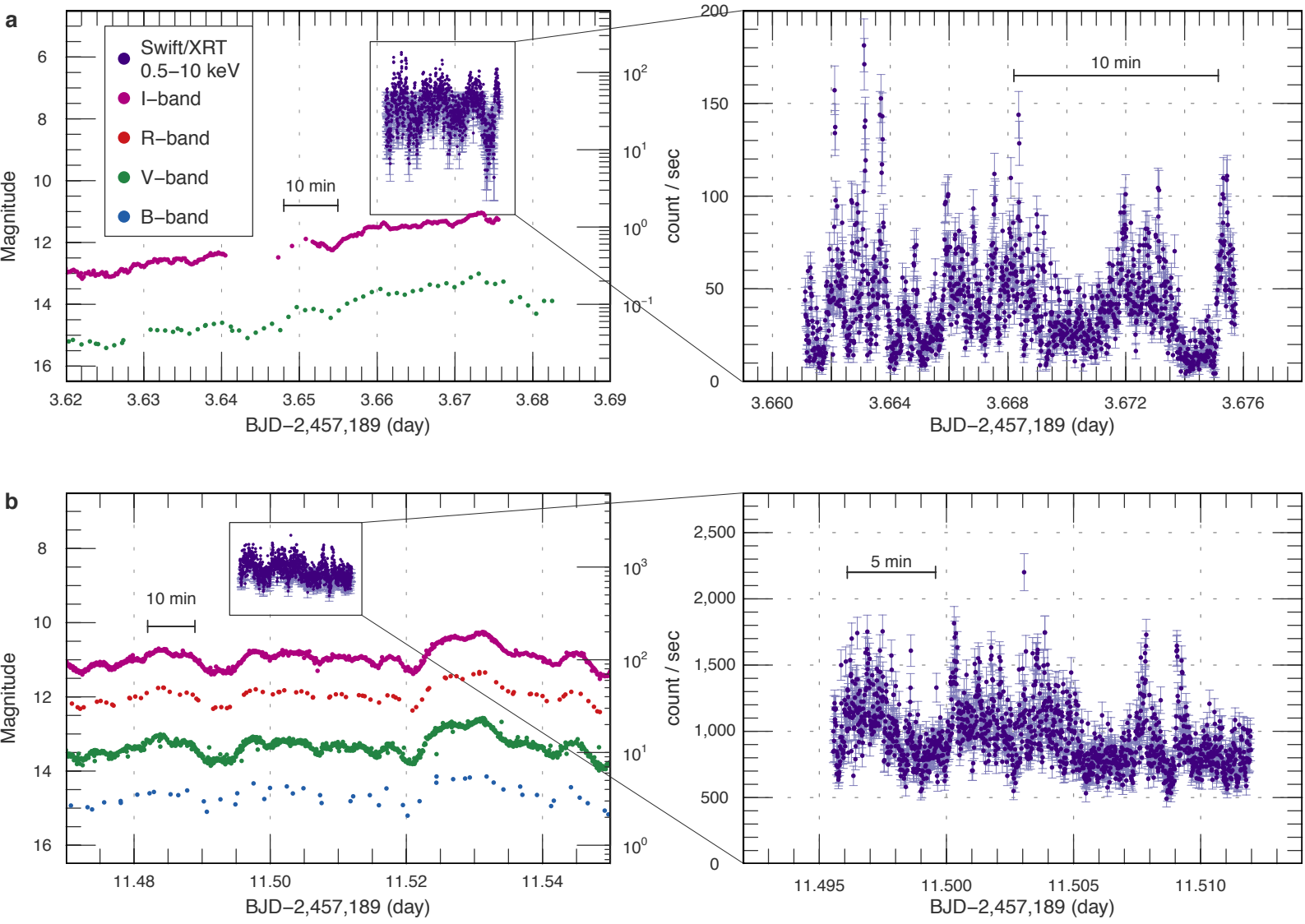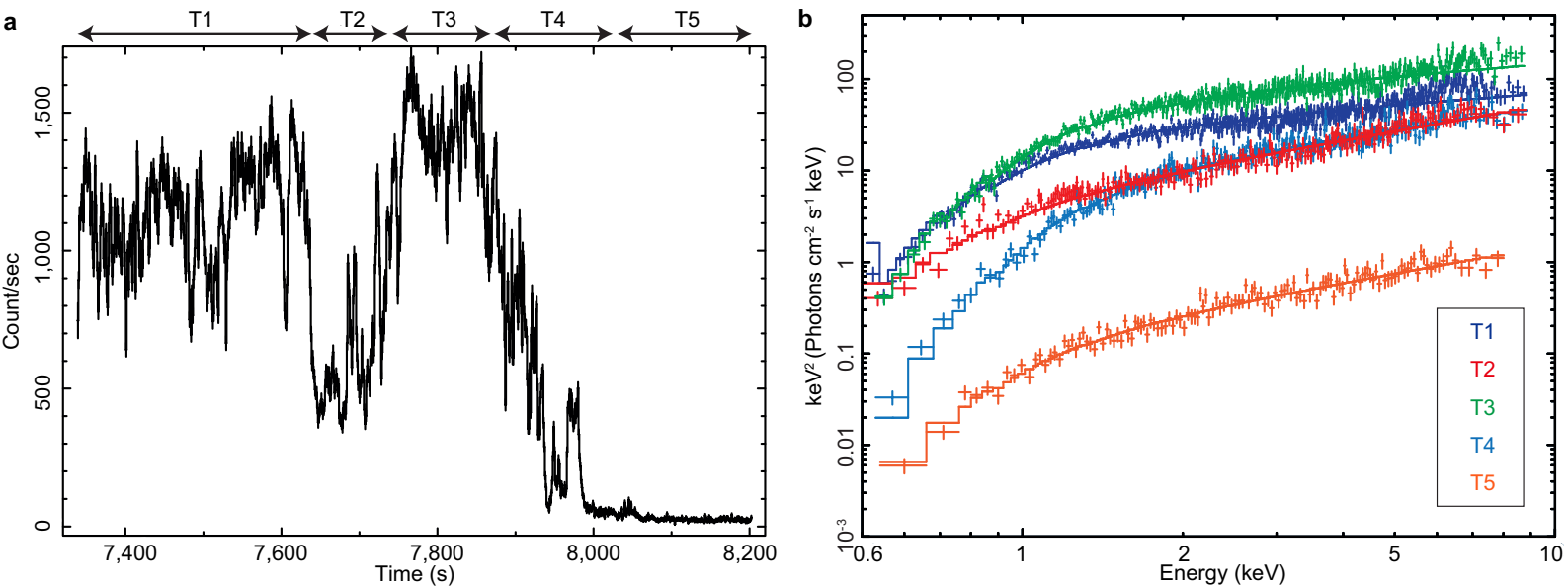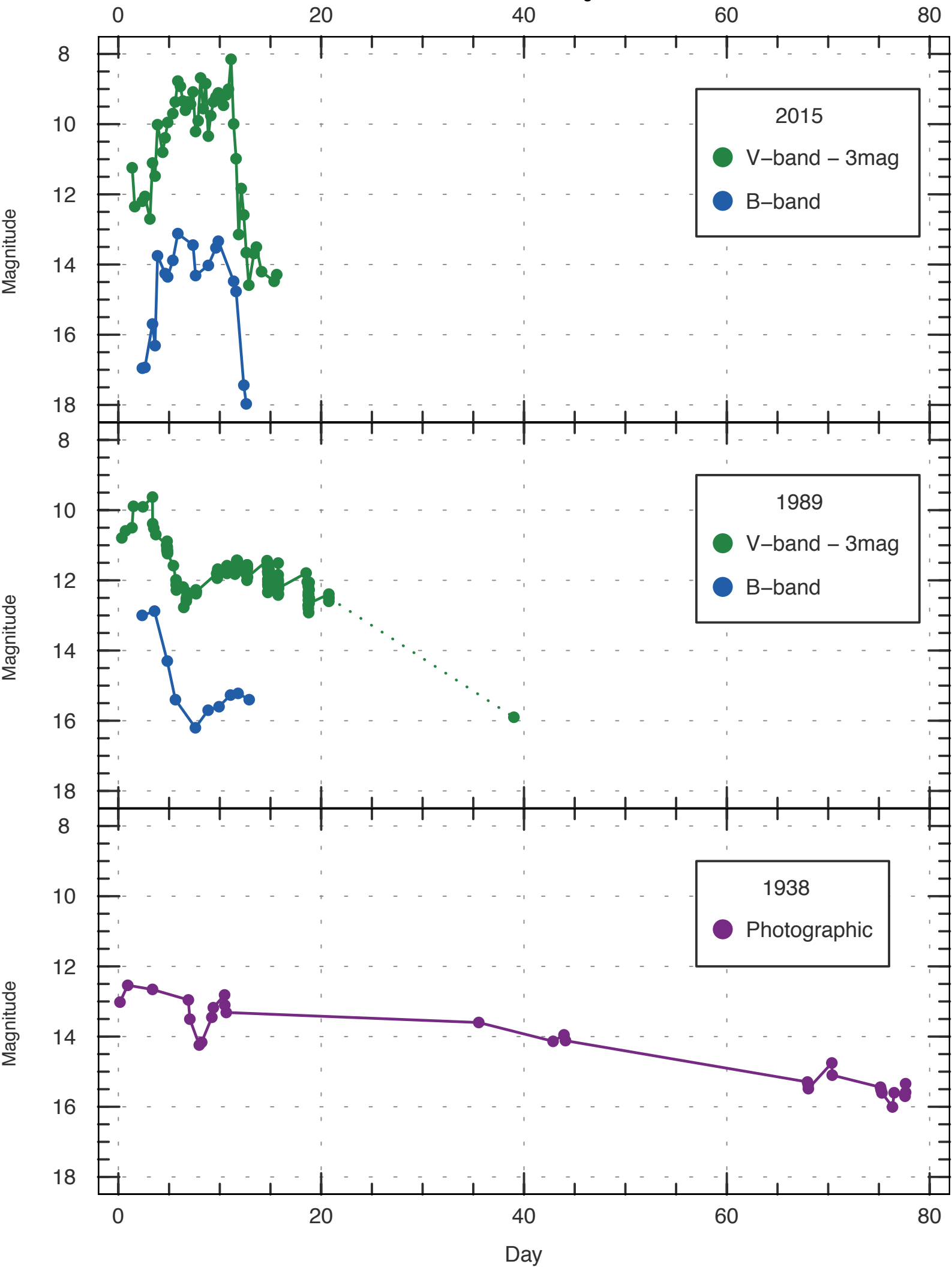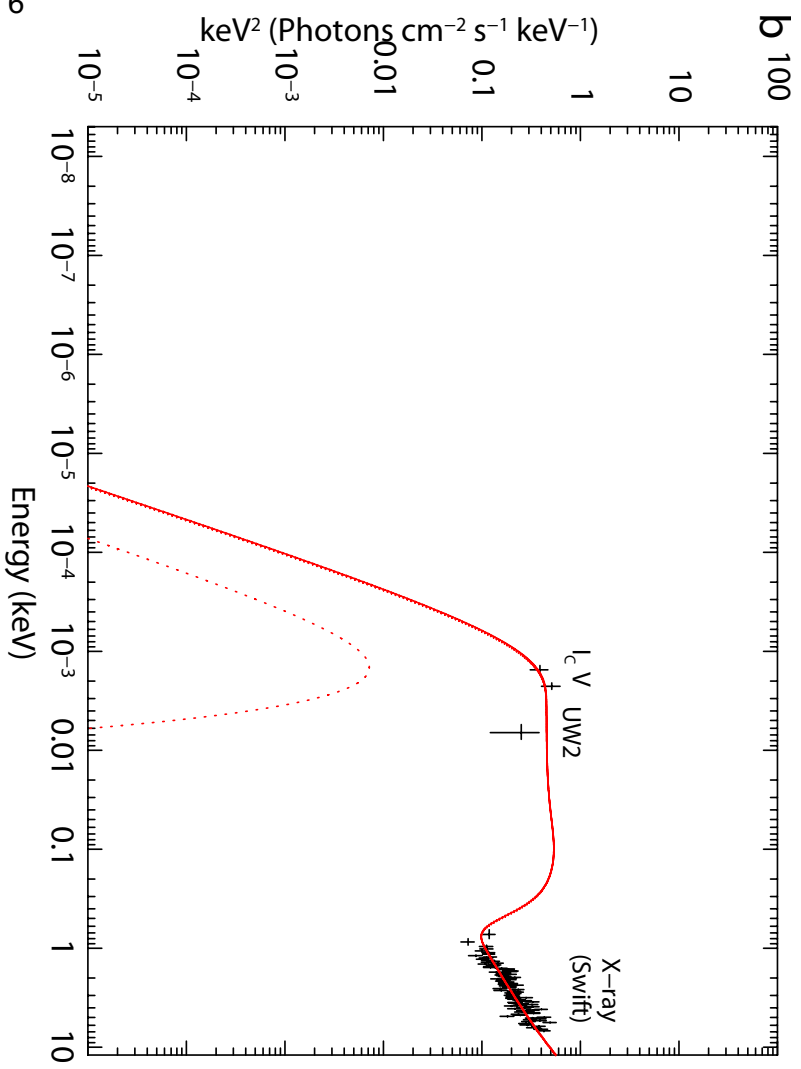| Start*	End*	Mag†	Error‡	N§	Obs‖	Band¶	Start*	End*	Mag†	Error‡	N§	Obs‖	Band¶
0.274	0.295	13.24	0.032	215	TAO	R	7.314	7.511	12.54	0.065	67	CRI	V
0.282	0.499	15.34	0.101	37	PZN	CR	7.314	7.512	11.45	0.060	66	CRI	R_C
0.386	0.426	15.18	0.036	86	PZN	R_C	7.315	7.511	10.36	0.061	65	CRI	I_C
0.386	0.426	14.31	0.040	20	CRI&PZN	R_C	7.422	7.588	10.52	0.011	1501	IMi	I_C
1.137	1.192	14.92	0.024	61	PZN	CR	7.427	7.670	11.35	0.035	1104	deM	I_C
1.274	1.398	13.93	0.086	20	PZN	R_C	7.675	7.802	10.81	0.012	1961	LCO	I_C
1.283	1.284	11.40	0.000	2	KW2	I_C	7.707	7.945	10.70	0.019	1003	SWI	I_C
1.283	1.284	12.50	0.000	2	KW2	V	7.744	7.907	12.98	0.036	350	GFB	V
1.283	1.284	11.95	0.068	2	KW2	B	8.030	8.300	10.22	0.020	535	KU1	I_C
1.551	1.670	13.48	0.029	191	deM	I_C	8.032	8.035	11.69	0.036	5	OKU	V
1.627	1.810	14.98	0.009	2430	LCO	CR	8.038	8.297	10.27	0.016	1022	OKU	I_C
2.109	2.517	15.07	0.024	224	PZN	CR	8.038	8.128	12.03	0.040	81	Ioh	CR
2.277	2.404	14.57	0.104	35	PZN	R_C	8.152	8.214	12.41	0.028	103	Wnm	cG
2.341	2.522	14.19	0.044	231	DPV	CR	8.360	8.543	9.95	0.015	68	CRI	I_C
2.354	2.529	15.41	0.056	158	DPV	V	8.394	8.619	10.41	0.011	623	Kai	I_C
2.354	2.529	14.12	0.049	158	DPV	R_C	8.419	8.671	10.17	0.012	1129	deM	I_C
2.380	2.505	17.19	0.075	61	Ter	B	8.709	8.859	13.42	0.036	413	RIT	V
2.380	2.505	15.52	0.072	61	Ter	V	8.969	9.043	10.87	0.019	296	Sac	I_C
2.381	2.506	14.33	0.062	61	Ter	R_C	8.993	9.154	10.55	0.024	608	Kis	I_C
2.406	2.524	14.65	0.024	354	Ter	CR	9.006	9.044	12.77	0.032	40	Sac	V
2.422	2.615	14.43	0.045	151	Kai	I_C	9.179	9.315	12.49	0.053	146	PZN	CR
2.423	2.609	14.43	0.045	147	Kai	R_C	9.224	9.229	12.59	0.149	5	OKU	V
2.446	2.669	13.46	0.021	667	deM	I_C	9.239	9.300	10.84	0.020	152	OKU	I_C
2.742	2.859	13.91	0.009	2652	LCO	CR	9.382	9.620	10.40	0.002	643	Kai	I_C
3.801	3.341	12.55	0.048	1216	TAO	R	9.414	9.595	10.24	0.003	428	NDJ	I_C
3.251	3.524	16.10	0.054	186	Ter	B	9.577	9.841	13.54	0.020	620	RIT	B
3.252	3.525	14.45	0.051	183	Ter	V	9.607	9.798	12.21	0.005	4709	LCO	V
3.252	3.524	13.41	0.044	177	Ter	R_C	9.635	9.828	10.13	0.010	1823	LCO	I_C
3.260	3.529	13.58	0.017	1278	Ter	CR	9.744	9.911	12.38	0.031	350	GFB	V
3.266	3.308	13.54	0.086	48	PZN	CR	10.027	10.028	11.90	0.018	3	Kis	V
3.271	3.307	13.64	0.091	40	PZN	R_C	10.029	10.201	10.54	0.011	837	Kis	I_C
3.410	3.489	15.80	0.095	38	CRI	B	10.387	10.619	10.46	0.020	611	Kai	I_C
3.411	3.488	14.36	0.071	37	CRI	V	10.415	10.670	10.38	0.013	1389	deM	I_C
3.411	3.488	13.17	0.062	37	CRI	R_C	10.744	10.910	11.99	0.010	349	GFB	V
3.411	3.489	12.01	0.058	37	CRI	I_C	11.182	11.300	9.41	0.012	99	KU1	I_C
3.419	3.588	14.48	0.048	189	RPc	V	11.291	11.298	10.55	0.003	112	TAO	R
3.428	3.553	14.52	0.056	128	Trt	V	11.339	11.514	10.51	0.018	406	DPV	I_C
3.430	3.519	12.25	0.023	597	IMi	I_C	11.348	11.554	13.10	0.014	730	Trt	V
3.435	3.673	12.47	0.020	1036	deM	I_C	11.372	11.515	13.15	0.019	335	DPV	V
3.525	3.650	12.64	0.075	37	COO	I_C	11.385	11.592	11.00	0.015	490	Kai	I_C
3.530	3.820	14.53	0.076	165	Kis	V	11.421	11.673	11.32	0.021	1314	deM	I_C
3.819	3.821	10.39	0.014	2	Kis	I_C	11.460	11.624	13.71	0.097	70	JSa	V
3.998	4.057	11.49	0.038	149	KU1	I_C	11.483	11.603	13.53	0.016	374	RJV	V
4.059	4.311	12.04	0.036	397	Mdy	R_C	11.590	11.679	14.43	0.014	730	LCO	V
4.187	4.316	11.88	0.022	169	TAO	R	11.679	11.834	12.95	0.008	3859	LCO	I_C
4.435	4.673	11.66	0.021	1089	deM	I_C	12.228	12.232	15.49	0.139	5	OKU	V
4.546	4.649	13.41	0.041	82	Kis	V	12.234	12.271	12.95	0.028	177	TAO	R
4.579	4.637	11.32	0.008	1416	LCO	I_C	12.302	12.334	13.81	0.011	311	TAO	R
4.976	4.978	12.14	0.034	5	Kis	V	12.386	12.611	13.89	0.025	484	Kai	I_C
4.979	4.981	10.04	0.004	3	Kis	I_C	12.405	12.670	14.08	0.022	640	deM	I_C
5.070	5.223	11.19	0.042	254	Mdy	R_C	12.484	12.599	16.87	0.031	237	RJV	V
5.426	5.481	12.75	0.054	36	CRI	B	13.058	13.314	15.81	0.013	211	Mdy	R_C
5.427	5.481	13.96	0.057	36	CRI	V	13.199	13.334	15.97	0.048	1772	TAO	R
5.427	5.480	11.66	0.048	35	CRI	R_C	13.382	13.594	14.28	0.014	467	Kai	I_C
5.427	5.480	10.57	0.044	36	CRI	I_C	13.415	13.670	14.08	0.022	640	deM	I_C
5.448	5.633	10.45	0.010	840	deM	I_C	13.438	13.473	13.91	0.040	93	NDJ	I_C
5.595	5.670	10.25	0.020	25	COO	I_C	14.014	14.021	17.21	0.075	5	OKU	V
5.724	5.954	9.85	0.007	920	SWI	I_C	14.026	14.168	14.75	0.022	97	OKU	I_C
5.745	5.911	11.69	0.011	346	GFB	V	14.043	14.276	14.70	0.016	361	Kis	I_C
5.923	5.949	10.32	0.013	24	COO	I_C	14.379	14.499	17.00	0.030	52	Trt	CV
6.011	6.015	12.51	0.016	5	OKU	V	14.421	14.565	14.85	0.012	152	RPc	I_C
6.019	6.076	10.27	0.005	154	OKU	V	14.422	14.614	14.56	0.007	248	NDJ	I_C
6.146	6.157	10.01	0.050	4	KW2	I_C	14.504	14.517	17.15	0.114	5	Trt	V
6.146	6.157	12.02	0.121	4	KW2	V	14.601	14.810	15.56	0.003	1830	LCO	CR
6.146	6.157	13.15	0.159	2	KW2	B	15.166	15.276	16.92	0.234	664	TAO	R
6.182	6.281	10.55	0.048	129	Aka	R_C	15.356	15.549	16.04	0.007	244	DPV	CR
6.210	6.280	12.41	0.060	64	Aka	V	15.364	15.550	17.41	0.024	42	DPV	V
6.293	6.554	11.31	0.030	85	CRI	R_C	15.434	15.559	14.84	0.017	81	RPc	I_C
6.295	6.550	12.30	0.037	83	CRI	V	15.694	15.762	14.45	0.008	166	SWI	I_C
6.346	6.428	11.84	0.028	93	PZN	R_C	16.092	16.142	14.60	0.397	5	TAO	R
3.356	6.543	9.94	0.011	412	DPV	I_C	16.302	16.377	16.07	0.013	26	PZN	CR
6.363	6.521	12.25	0.010	572	Trt	V	16.320	16.525	14.44	0.010	129	CRI	I_C
6.369	6.406	10.09	0.008	334	DPV	I_C	16.344	16.435	14.50	0.012	52	DPV	I_C
6.430	6.615	12.38	0.022	418	RJV	V	16.516	16.530	14.44	0.030	6	RPc	I_C
6.584	6.827	12.65	0.005	5910	LCO	V	16.680	16.937	14.36	0.006	335	SWI	I_C
6.592	6.861	10.54	0.012	794	RIT	I_C	17.358	17.518	14.48	0.006	218	DPV	I_C
6.717	6.944	10.36	0.007	942	SWI	I_C	17.418	17.671	14.78	0.006	309	deM	I_C
6.745	6.912	12.35	0.010	347	GFB	V	17.440	17.575	14.62	0.014	43	RPc	I_C
6.919	6.950	10.35	0.076	24	COO	I_C	18.297	18.336	17.37	0.254	470	TAO	R
7.056	7.057	13.27	0.010	3	Kis	V	19.328	19.332	16.45	0.258	68	TAO	R
7.057	7.137	10.55	0.019	295	Kis	V	19.403	19.451	14.82	0.011	33	DPV	I_C
7.115	7.147	10.01	0.018	45	Aka	R_C	19.423	19.498	14.79	0.026	17	RPc	I_C
7.144	7.150	9.87	0.016	18	KW2	I_C	19.712	19.761	16.61	0.008	60	GFB	CV
7.144	7.150	11.76	0.068	18	KW2	V	20.435	20.592	14.98	0.008	90	RPc	I_C
7.144	7.150	13.44	0.184	2	KW2	B	21.023	21.031	15.34	0.012	10	RPc	I_C
7.313	7.512	13.79	0.063	67	CRI	B							

∗ JD−2457189.　† Mean magnitude.　‡ 1σ of mean magnitude.　§ Number of observations.

‖ Observer's code: PZN (IKI GRB follow up network), CRI (Crimean Observatory Team), deM (Enrique de Miguel), DPV (Pavol A. Dubovsky), Ter (Terskol Observatory), Kai (Kiyoshi Kasai), NDJ (Nick James), RPc (Roger D. Pickard), Trt (Tam´as Tordai), COO (Lew Cook), Kis (Seiichiro Kiyota), KU1 (Kyoto U. Team), Mdy (Yutaka Maeda), LCO (Colin Littlefield), RIT (Michael Richmond), RJV (Ruiz F. Javier), GFB (William Goff), SWI (William L. Stein), OKU (Osaka Kyoiku U. team), Sac (Atsushi Miyashita), IMi (Ian Miller), TAO (TAOS Team) KW2 (Hiroyuki Maehara), Aka (Hidehiko Akazawa) Wnm (Kenji Hirosawa) JSa (Josep Lluis)

¶ Filter. B, V , R_C, I_C are the standard Johnson-Cousins system. "CR" and "CV" mean unfiltered CCD photometry adjusted R and V for the zero point, respectively. "cG" means green (G) channel output in digital single-lens reflex camera, which gives an approximate response close to V [78] (Kloppenborg et al. 2012).

Extended Data Table 2

CODE	Telescope (& CCD)	Observatory (or Observer)	Site
PZN	1m Zeiss-1000 Tien Shan +Apogee Alta	Astronomical Observatory	Almaty, Kazakhstan
	40cm ORI-40+FLI ML09000	ISON-Khureltogot	Mongolia
	70cm+FLI AS-32+FLI IMG6303E	Abastumani observatory	Georgia
CRI	1.25m AZT-11+FLI ProLine PL230	Crimean astrophysical observatory	Crimea
	38cm K-380+Apogee E47	Cremean astrophysical observatory	Crimea
deM	35cm SC+QSI-516wsg	Observatorio Astronomico del CIECEM	Huelva, Spain
DPV	28cm SC+MII G2-1600	Astronomical Observatory on Kolonica	Slovakia
	35cm SC+MII G2-1600	Astronomical Observatory on Kolonica	Slovakia
	VNT 1m+FLI PL1001E	Astronomical Observatory on Kolonica	Slovakia
Ter	Zeiss-600 60cm+SBIG STL-1001E	Terskol Observatory	Russia
	S2C 35cm	Terskol Observatory	Russia
Kai	28cm SC+ST7XME	Kiyoshi Kasai	Switzerland
NDJ	28cm SC+ST9XE	Nick James	UK
RPc	FTN 2.0m+E2V 42-40	LCOGT*	Hawaii, USA
	35cmSC+SXV-H9 CCD	Roger D. Pickard	UK
Trt	25cm ALCCD5.2 (QHY6)	Tamás Tordai	Budapest, Hungary
COO	T07[†] 43cm+STL-1100M	AstroCamp Observatory	Nerpio, Spain
	T21[†] 43cm+FLI-PL6303E	iTelescope.Net Mayhill	New Mexico, USA
	T11[†] 50cm+FLI ProLine PL11002M	iTelescope.Net Mayhill	New Mexico, USA
Kis	25cm SC+Alta F47	Seiichiro Kiyota	Kamagaya, Japan
	T18[†] 32cm+STXL-6303E	AstroCamp Observatory	Nerpio, Spain
	T5[†] 25cm+ST-10XME	iTelescope.Net Mayhill	New Mexico, USA
	T24[†] 61cm+FLI-PL09000	Sierra Remote Observatoy	California, USA
KU1	40cm SC+ST-9XEI	Kyoto U. Team	Kyoto, Japan
Mdy	35cm SC+ST10XME	Yutaka Maeda	Nagasaki, Japan
LCO	60cm+Apogee Alta U42 CCD	Van Vleck Observatory	Connecticut, USA
	40cm+SBIG STL-6303	Van Vleck Observatory	Connecticut, USA
RIT	30cm+ST-9E	RIT Observatory	New York, USA
RJV	LX200R 40cm+ST8 XME	Observatorio de Cantabria	Spain
GFB	CDK 50cm+Apogee U6	William Goff	California, USA
SWI	C14 35cmSC+ST10XME	William L. Stein	New Mexico, USA
OKU	51cm+Andor DW936N-BV	OKU Astronomical Observatory	Osaka, Japan
Sac	20cmL+ST-7XMEi	Atsushi Miyashita	Tokyo, Japan
IMi	35cm SC+SXVR-H16	Furzehill Observatory	UK
TAO	TAOS-B[‡] 50cm+SI800 E2V47-20	Lulin Observatory	Taiwan
	TAOS-D[‡] 50cm+SI800 E2V47-20	Lulin Observatory	Taiwan

* Las Cumbres Observatory Global Telescope Network

† itelescope.net

‡ The Taiwanese-American Occultation Survey (TAOS) [80] (Alcock et al. 2003); [33] (Lehner et al. 2009); [81] (Zhang et al. 2013)

Extended Data Table 3

	V404 Cyg	GRS 1915+105	IGR J17091-3624	Rapid Burster	V4641 Sgr
Orbital period [d]	6.47129(7) (ref. 83)	33.85(16) (ref. 20)	>4 (ref. 84)	–	2.81678 (ref. 23)
Compact object	BH	BH	BH	NS	BH
Spectrum of the secondary	K3III (ref. 7)	K–M (ref. 20)	–	–	B9III (ref. 23)
M_1 ($M_\odot$)	9.0(0.6) (ref. 7)	10.1(0.6) (ref. 85)	11.8–13.7 (ref.86)	1.1(0.3) (ref. 87)	7.1(0.3) (ref. 88)
$q = M_2/M_1$ **(Mass ratio)**	0.06 (ref. 7)	0.042(0.024) (ref. 20)	–	–	0.45(0.05) (ref. 88)
i **[deg] (Inclination angle)**	67(3) (ref. 7)	66(2) (ref. 89)	50–70 (ref. 90)	–	72.3(4.1) (ref. 88)
V **magnitude minimum**	18.4 (ref. 91)	–	–	–	13.8 (ref. 88)
V **magnitude maximum**	10.9	–	–	–	8.8 (ref. 41)

NOTE: M_1 and M_2 represent mass of the central object and that of the secondary star, respectively.